Civil Engineering Infrastructures Journal xx,xx

DOI: 10.22059/ceij.2025.391455.2263

Technical Notes

Analysis of Buckling Problems of Trigonometric Shear Deformable Rectangular Plates: Variational Formulation and Solutions for Simply Supported Plate Buckling Problems using Galerkin Method

Charles Chinwuba Ike
Department of Civil Engineering, Enugu State University of Science and Technology
Email: charles.ike@esut.edu.ng

Received: 03/03/2025

Revised: 08/08/2025

Accepted: 04/09/2025

Abstract

This work considered transverse shear deformations in the derivation of thick plate buckling problem. Trigonometric shear form functions were derived using first principles to ensure that the plate surfaces are free of transverse shear strains. Hence shear correction factors were not needed. The first variation of the total energy functional was made to vanish to establish the differential equations of stability (DES). Exact displacement shape functions were used in the Galerkin variational method (GVM) to determine analytical and numerical solutions. The GVM simplified the DES to a homogeneous algebraic eigenvalue problem. The condition for nontrivial solutions was used to determine the characteristic buckling equation, with the least eigenvalue yielding the critical buckling load, which were determined for uniaxial and biaxial compressive loads studied. The work was validated by favourable comparisons with previous shear deformation plate results. It was also found that the critical buckling loads were significantly lower than those predicted by classical Kirchhoff thin plate theory (CPT) confirming that CPT overestimates the critical buckling loads of thick plates for all aspect ratios. The GVM is mathematically rigorous as the boundary conditions are satisfied as well as the DES, making the method exact within the theoretical framework considered.

Keywords: Trigonometric Shear Deformable Plate, Galerkin Variational Method, Critical Buckling Load

1. Introduction

Plates are vital structural elements characterized by in-plane dimensions that are much larger than their transverse dimensions. They are found in marine, aeronautical, ship and building structures. When they are subject to in-plane compressive loads on their mid-surface planes, they may deform out of their plane resulting in a wave-like pattern across their surfaces. This instability called buckling can escalate to structural failure, making buckling analysis vital, especially where plates face complex and variable load and boundary conditions. Plate buckling is primarily caused by in-plane compressive forces acting on the middle surface of the plate. When a plate is loaded beyond its elastic stability limit, it attains a critical stress point at which bifurcation occurs leading to buckling [Prabowo et al, 2023].

The buckling behaviour of plates depends on the elastic properties, geometry, edge supports and loading conditions. When the plate thickness (h) to least in-plane dimension (a) is less than 0.05, the plate is thin. Otherwise, the plate is moderately thick or thick. Plates are classified according to their elastic properties as homogeneous when their properties are the same over the plate region, and non-homogeneous otherwise. They are anisotropic when their properties vary with direction at a point, and isotropic, otherwise [Fu and Wang, 2022; Onodagu et al 2023; Godwin et al, 2023].

Kirchhoff derived the CPT for thin plates using the orthogonality hypothesis requiring that straight normal planes originally orthogonal to the middle surface remain straight and orthogonal to the middle surface after deformation. Plate buckling solutions are also presented in Timoshenko and Gere (1961). This means that transverse shear deformations are neglected in the CPT limiting its use to thin plates where transverse shear deformations are negligible. Thin plate buckling has been extensively investigated using several methods including Galerkin variational methods, integral transformation methods and Ritz methods.

Efforts at improvements to the thin plate theories led to the formulations of displacement based shear deformation theory by Mindlin (1951). Mindlin plate theory (MPT) is a first order shear deformation theory (FSDT) which yields constant transverse shear strains across the thickness, thus violating the transverse shear strain-free conditions at the surfaces.

Shear correction factors were introduced into the MPT to correct this violation but there is no systematic mathematically rigorous means to determine the correction factors, rendering it a defect to the MPT.

Flexural and buckling studies of Mindlin plates were done by Ike (2025a, 2025b, 2025c) using double Fourier series method, Ritz variational method and exact method respectively.

Further efforts to improve the accuracy of thick plate analysis led to the developments of other FSDTs, higher order shear deformation plate theories (HSDTs), and refined plate theories (RPTs). Hashemi et al (2008) presented exact buckling solutions for rectangular Mindlin plates. Ullah et al (2019) utilized a two-dimensional (2D) finite sine integral transformation method for the closed-form buckling solutions of rectangular Kirchhoff plate with rotationally restrained edges. Unlike the conventional inverse / semi-inverse methods, the transform method did not require a prior determination of the deflection basis functions which is provided in the integral kernel function used. It also yields the direct solution of the governing differential equation (GDE) in the transform domain, ultimately converting the GDE to a set of linear algebraic eigenvalue problem. Their solutions were validated using finite element ABAQUS software solution.

Ike (2023a) used double finite sine transformation method (DFSTM) to develop closed form buckling solutions for single variable thick plate buckling problems. The DFSTM adopted, transformed the GPDE to algebraic eigenvalue equations from which the critical buckling loads were found for simply supported boundary conditions (BCs). The DFSTM solutions were found to be exact.

Deepak et al (2021, 2022) studied buckling analysis of thick plates using a single variable third order shear deformation plate theory. Their study used a single displacement function to formulate the thick plate buckling problem as one governing partial differential equation (GPDE). The GPDE is similar in form to equations of CPT. The GPDE satisfied shear stress-free conditions at the top and bottom surfaces, and obviates the need for shear correction. The solution methods for CPT are useful for solving the GPDE due to the close resemblance of both equations. They presented critical buckling solutions of simply supported rectangular plates and validated their results by agreeable results with other previous results. Wang et al (2025) also presented a single variable third order shear deformable model for free vibration analysis.

Shimpi et al (2018) have also presented FSDT using one unknown displacement variable for rectangular thick homogeneous, isotropic plates. Malikan and Nguyen (2018) developed a single variable first-order shear deformable plate buckling theory (SVSDT) using Eringen's nonlocal elasticity concepts for buckling. Their work was aimed at correcting the inherent errors of the first order shear deformation theory (FSDT) which result in constant shear stress across the thickness.

Khalfi et al (2021) developed buckling solutions for thick isotropic and orthotropic plates based on the two-variable refined plate theory (2VRPT). The 2VRPT assumed sinusoidal functions of thickness for transverse shear stresses and strains across the depth, such that transverse shear stress-free conditions are satisfied on top and bottom surfaces. The domain equations were derived using the principles of virtual displacements. The non-linear Von-Karman kinematic equations were considered for the kinematics relations. They obtained analytical solutions for simply supported rectangular plates under in-plane loading using Navier's double trigonometric series method.

Onyeka et al (2022) presented buckling analysis of thick plate using a direct variational method based on the minimization of the total potential energy of the buckling plate. Their work considered transverse shear deformation and used two cases of trigonometric basis functions and polynomial basis functions. They obtained critical buckling loads that were higher than those of refined plate theories by 7.70%; but different from exact elasticity theories by 1%.

Srivinas and Rao (1969) studied the buckling of rectangular thick plates and derived exact buckling solutions for cases of uniaxial compression loading of simply supported plates. Reddy (1984) developed a higher-order shear deformation theory of laminated composite plates that yields a parabolic distribution of transverse shear strains across the plate depth. Reddy's theory satisfies the transverse shear strain free-conditions at the top and bottom surfaces of the plate and does not need transverse shear stress correction factors. It was found that Reddy's theory gives more accurate values of deflections and stresses than the first-order shear deformation theory. Reddy and Phan (1985) have presented buckling solutions for thick plates based on HSDT.

Boureda et al (2016) proposed a new four variable refined plate theory for the stability analysis of thick plates made of isotropic and orthotropic materials. Unlike

the HSDT and FSDTs, the model used a novel displacement field with unknown integral terms and has only four unknown variables. The principle of virtual work was used to derive the GPDE. Their work presented buckling solutions for simply supported rectangular plates under uniaxial compression using the Navier series method. Their results were validated by favourable comparison to the previous results by FSDT.

Moslemi et al (2016a) used displacement potential functions to simplify the governing equations of plate buckling to two PDEs; one is second order and the other is of fourth order. The PDEs were formulated for rectangular isotropic plates of any depth and were thus applicable to thick plates. The GPDEs were solved using separation of variables method and made to satisfy BCs to yield mathematical solutions for linear elastic buckling of simply supported rectangular thick plates under in-plane uniaxial or biaxial static loads. Critical buckling loads were found to agree with previous results in the literature. In another study, Moslemi et al (2016b) presented stability solutions for rectangular thick biaxially loaded transversely isotropic plates.

Sayyad and Ghugal (2014) utilized a novel trigonometric shear and normal deformation theory to solve thick plates buckling problems under uniaxial and biaxial compression. Their theory yields a cosine function for the distribution of transverse shear strain across the plate depth. It also satisfied the transverse shear stress-free conditions at the plate surfaces, and does not require transverse shear stress correction factors. The principle of virtual work was used to formulate the GPDE and BCs. Their study gave closed-form solutions using Navier double trigonometric series method for the stability analysis of simply supported, isotropic, orthotropic and laminated composite rectangular plates under uniaxial and biaxial compressive loads. Their results were validated by favourable comparisons with results of FSDT, HSDT and exact three-dimensional (3D) elasticity theory. Their study found that their results were in good agreement with HSDT and elasticity theory results.

Sayyad et al (2022) presented a refined simple FSDT for the stability analysis of orthotropic and laminated composite plates. Their work led to a quadratic variation of transverse shear strains across the plate depth and satisfies the transverse shear stress-free boundary conditions at the plate surfaces. The equations were free of shear correction factors, and were derived using the principle of virtual work. They obtained satisfactory solutions using Navier method for simply supported rectangular plates under uniaxial and biaxial compressive loads.

Mohseni and Naderi (2023) presented closed form solutions for buckling analysis of thick porous FG plates under in-plane loads using higher order shear and normal deformable plate models. Buckling load solutions were obtained for simply supported rectangular plates using Legendre orthonormal polynomials and Naviers method.

Kim et al (2009) developed refined plate buckling model for composite and isotropic materials using two unknown displacement variables. They used the virtual work principle to derive the governing equation and the Navier series method to develop solutions for simply supported plate buckling problems.

Kim et al (2009) formulated a two-variable refined plate theory for the buckling analysis of thick plates. They used refined formulations of the displacements fields as the sum of bending and shear components of each of the components to develop equations in terms of two unknown variables. They obtained accurate critical buckling load solutions for thick plates under uniform tensile load in the x-

direction and uniform compressive load in the *y* direction.

Jayabalen et al (2022) used various data sets compiled from relevant literature on plates buckling and applied artificial intelligence techniques like Gene Expression Programming (GEP), Artificial Neural Network (AMT) and Evolutionary Polynomial Regression (EPR) to obtain critical buckling loads of steel plates. The models were compared and ANN model had an R^2 of 0.986 with an average error of 10.4%.

Hassan and Kurgan (2019) used ANSYS finite element software for the buckling studies of homogeneous and FG plates. Various elements (shell elements, solid elements, tetrahedral elements brick elements and solid-shell elements) were studied. Various boundary conditions wree also studied using ANSYS.

Gunjal et al (2015) used a refined trigonometric shear deformation plate theory for the stability analysis of thick plates under uniform uniaxial and biaxial compression. Their work assumed a sinusoidal function in the depth coordinate to formulate the shear form function in the in-plane displacement and ensure that the top and bottom plate surfaces are free of transverse shear strains. The formulated equations have only two unknown displacements. The principle of virtual work was used to derive the GPDE and BCs. Navier's double series method was used to solve the resulting GPDE for simply supported plate under uniform uniaxial and biaxial compression loads. The solution method yielded an algebraic eigenvalue problem from which exact critical buckling load solutions were obtained for various aspect ratios (a/h) and ratios of the sides (b/a). Thai and Choi (2013) have also presented buckling solutions for thick plates using RPT.

Gajbhiye et al (2022) used a fifth order shear deformation plate theory that considers transverse and normal shear effects to study how transverse normal strains affect the buckling of thick plates. Their formulation satisfied the transverse shear stress-free conditions at the surfaces and did not need transverse shear correction. The principle of minimum potential energy was used to determine the GPDEs and BCs. They found solutions for simply supported thick plates that agreed with previous solutions.

Ike (2023b) developed from first principles, a third-order shear deformation plate bending formulation, but did not consider buckling. Su et al (2023) employed symplectic superposition method (SSM) to present a unified framework for flexural, buckling, and vibration solutions of rectangular Kirchhoff plates with four free edges. Their work considered isotropic and orthotropic materials. The advantage of SSM is the use of orthogonal series expansion of symplectic eigenvectors found from a Hamiltonian formulation of the governing differential equations. The orthogonality properties simplified the evaluation of the resulting integration problems and led to accurate solutions.

Kumar and Singh (2018) evaluated various HSDTs for modeling and buckling analysis of functionally graded material (FGM) plates using radial basis functions (RBF) based meshless method. The HSDTs considered accounted for shear deformation effects and were thus applicable to thick plates buckling. The formulation did not require shear correction factors as transverse shear stress-free conditions on the plate surfaces were satisfied. Accurate solutions using meshless method were obtained in their study.

Zargaripoor et al (2018) explored exact wave propagation approach for the first time to develop buckling solutions for thick rectangular plates modeled using third-order shear deformation plate theory (TSDT). The plate model used satisfied the transverse shear stress-free conditions at

the top and bottom surfaces, and had no need for shear correction. They considered plates with two opposite simply supported edges, while the other edges may be clamped or simply supported. They derived the characteristic equation using wave propagation methods and solved to obtain the buckling loads for different BCs considered.

Ike (2025e) derived an exponential shear deformable plate buckling model using variational calculus. The formulation ensured that the transverse shear stresses vanished at the plate surfaces, thus obviating the transverse shear correction factors. Minimization of the total potential energy functional was used to obtain the system of three coupled partial differential equations (PDEs). The Double Fourier series method was used in the paper to derive analytical buckling solutions for simply supported boundary conditions.

Exact critical buckling load solutions were obtained for square simply supported plates under uniaxial uniform compressive loads and for biaxial uniform compressive loads for different values of the Young's modulus – and Poisson ratio.

Despite the quantum of studies done so far on thick plate buckling investigations, very few have focused on development of the governing differential equations of stability using a first principles variational formulation method. Still, few researchers have attempted to derive analytical and numerical solutions using the Galerkin variational method (GVM).

In this study, the variational formulation of the thick plate buckling problem is done using a first principles approach and the resulting system of GPDE is solved using GVM. The work presents both analytical solutions and numerical solutions for the case of simply supported rectangular thick plate subjected to: (i) uniaxial compressive load in the x direction (ii) uniaxial compressive load in the y direction, and (iii) biaxial compressive load in both the x and y directions.

The GVM is adopted in this work because:

(i) it uses the displacement shape functions that satisfies the BCs as the integral kernel functions in constructing the Galerkin variational functional (GVF) for the problem.

(ii) when the displacement shape functions are orthogonal functions as is the case for Dirichlet boundary conditions, the orthogonality properties simplify the resulting integration problems.

(iii) the GVM yields exact solutions when the exact shape functions are used in formulating the GVF.

2. Theoretical Framework

The thick plate buckling problem considered as shown in Figure 1 is rectangular, with length a, width b, and thickness h. The origin of coordinates is shown as point O in Figure 1. Hence the plate domain is: $0 \le x \le a$, $0 \le y \le b$, $-h/2 \le z \le h/2$, where x, y, z are the Cartesian coordinates.

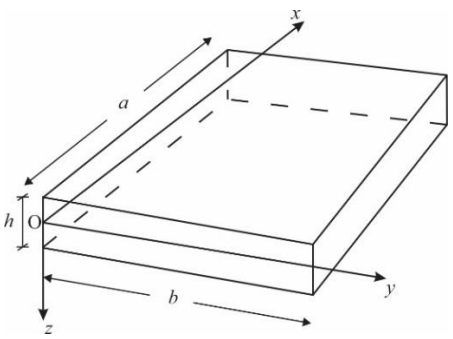

Figure 1: Thick plate considered

The thick plate is subjected to uniaxial and biaxial compressive loads as shown in Figures 2(i), 2(ii) and 2(iii).

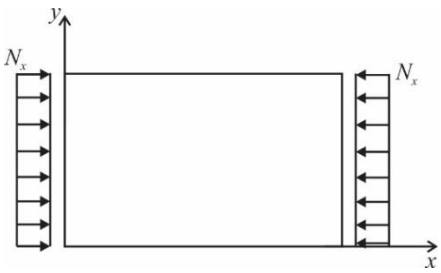

Figure 2(i): Thick plate under uniaxial compressive force N_x in the x direction

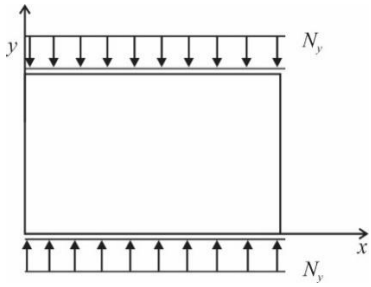

Figure 2(ii): Thick plate under uniaxial compressive force N_y in the y direction

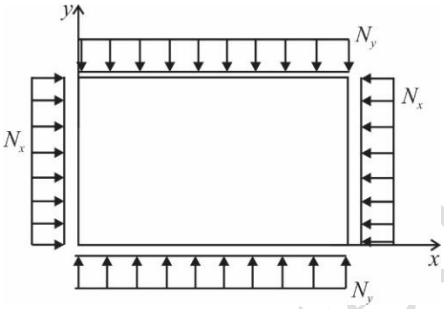

Figure 2(iii): Thick plate under biaxial compressive forces N_x, N_y

A thick plate subjected to in-plane uniform tensile load in the x-direction and in-plane uniform compressive load in the y direction as shown in Figure 2(iv) is further considered.

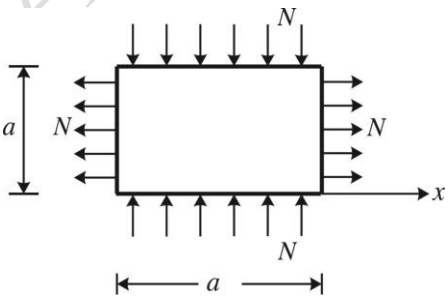

Figure 2(iv) Thick square plate subjected to uniform force N in the x-direction and uniform compressive force N in the y direction

Basic assumptions

These are:

(i) the plate is a flat plate, and all the compressive loads act in the middle plane.

(ii) the loads are static and do not change in magnitude or direction.

(iii) the plate material is linear elastic, isotropic and homogeneous.

(iv) the transverse normal stress in the z direction at the middle plane is zero, $\sigma_{zz} = 0$.

(v) the transverse deflection w at any point on the middle surface ($z = 0$) is the sum of the components due to bending deformation (w_b) and transverse shear effects (w_s). Thus $w(x, y, z = 0) = w_b(x, y, z = 0) + w_s(x, y, z = 0)$

(vi) the distribution of transverse shear stress across the plate thickness is assumed to follow trigonometric function in line with the assumption that the model to be derived in this study is a trigonometric shear deformation model.

Displacement components

The x, y, z components of the displacement at any point on the plate are $u(x, y, z)$, $v(x, y, z)$, $w(x, y, z)$ where

$$u(x, y, z) = -z\frac{\partial w}{\partial x} + f(z)\frac{\partial w_s}{\partial x}$$

$$v(x, y, z) = -z\frac{\partial w}{\partial y} + f(z)\frac{\partial w_s}{\partial y} \qquad (1)$$

$$w(x, y, z) = w(x, y, z = 0)$$

$f(z)$ is a function that defines the transverse shear stress distribution across the thickness. In this work $f(z)$ is derived to ensure that the transverse shear strains γ_{xz}, γ_{yz} vanish at the plate's top and bottom surfaces, where $z = \pm 0.5h$. It is also

derived such that $u(x, y, z = 0) = 0$; $v(x, y, z = 0) = 0$; and thus $f(z = 0) = 0$.

Strains

The in-plane normal strains $\varepsilon_{xx}, \varepsilon_{yy}$, and transverse normal strain ε_{zz} and shear strains $\gamma_{xy}, \gamma_{xz}, \gamma_{yz}$ are obtained using the kinematic relations of linear elasticity theory.

$$\varepsilon_{xx} = -z\frac{\partial^2 w}{\partial x^2} + f(z)\frac{\partial^2 w_s}{\partial x^2}$$

$$\varepsilon_{yy} = -z\frac{\partial^2 w}{\partial y^2} + f(z)\frac{\partial^2 w_s}{\partial y^2} \quad (2)$$

$$\varepsilon_{zz} = 0$$

$$\gamma_{xy} = -2z\frac{\partial^2 w}{\partial x \partial y} + 2f(z)\frac{\partial^2 w_s}{\partial x \partial y}$$

$$\gamma_{xz} = f'(z)\frac{\partial w_s}{\partial x}$$

$$\gamma_{yz} = f'(z)\frac{\partial w_s}{\partial y}$$

It is required that,

$$\gamma_{xz}(z = \pm h/2) = 0; \ \gamma_{yz}(z = \pm h/2) = 0 \quad (3)$$

Hence $f'(z = \pm h/2) = 0$ (4)

For trigonometric formulation that is adopted in this work, based on assumption (vi),

$$f'(z) = \cos a_1 z + \sin a_2 z \quad (5)$$

Since $f'(z = \pm h/2) = 0$

$f'(z)$ has to be an even function.

Hence, $a_2 = 0$ (6)

and $f'(z) = \cos a_1 z$ (7)

Using the transverse shear stress-free conditions, $\tau_{xz}(z = \pm 0.5h) = 0;$ and $\tau_{yz}(z = \pm 0.5h) = 0,$ it is obtained that:

$$f'(z = \pm h/2) = \cos\left(\frac{\pm a_1 h}{2}\right) \quad (8)$$

Solving from Equation (4),

$$\pm\frac{a_1 h}{2} = \cos^{-1} 0 \quad (9)$$

$$\pm\frac{a_1 h}{2} = (2n+1)\frac{\pi}{2}$$

where n takes the value of any integer

$$a_1 = \frac{\pi(2n+1)}{h} \quad (10)$$

$$a_1 = \frac{\pi}{h} \qquad (\text{for } n = 0) \quad (10a)$$

Hence, $f'(z) = \cos\frac{\pi z}{h}$ (11)

Hence,

$$\gamma_{xz} = \cos\left(\frac{\pi z}{h}\right)\frac{\partial w_s}{\partial x} \quad (12)$$

$$\gamma_{yz} = \cos\left(\frac{\pi z}{h}\right)\frac{\partial w_s}{\partial y} \quad (13)$$

Integrating Equation (11) with respect to z,

$$f(z) = \frac{h}{\pi}\sin\left(\frac{\pi z}{h}\right) + c_0 \quad (14a)$$

where c_0 is an integration constant.

For $f(z = 0) = 0$, $c_0 = 0$, and

$$f(z) = \frac{h}{\pi}\sin\left(\frac{\pi z}{h}\right) \quad (14b)$$

Stresses

The normal stresses $\sigma_{xx}, \sigma_{yy}, \sigma_{zz}$ are

$$\sigma_{xx} = \frac{E}{1-\mu^2}\left(-z\frac{\partial^2 w}{\partial x^2} + f(z)\frac{\partial^2 w_s}{\partial x^2} + \mu\left(-z\frac{\partial^2 w}{\partial y^2} + f(z)\frac{\partial^2 w_s}{\partial y^2}\right)\right) \quad (15)$$

$$\sigma_{yy} = \frac{E}{1-\mu^2}\left(-z\frac{\partial^2 w}{\partial y^2} + f(z)\frac{\partial^2 w_s}{\partial y^2} + \mu\left(-z\frac{\partial^2 w}{\partial x^2} + f(z)\frac{\partial^2 w_s}{\partial x^2}\right)\right) \quad (16)$$

$$\sigma_{zz} = 0 \quad (17)$$

where E is the Young's modulus, μ is the Poisson's ratio

$$\tau_{xy} = G\left(-2z\frac{\partial^2 w}{\partial x \partial y} + 2f(z)\frac{\partial^2 w_s}{\partial x \partial y}\right) \quad (18)$$

$$\tau_{xz} = G\cos\left(\frac{\pi z}{h}\right)\frac{\partial w_s}{\partial x} \quad (19)$$

$$\tau_{yz} = G\cos\left(\frac{\pi z}{h}\right)\frac{\partial w_s}{\partial y} \quad (20)$$

where G is the shear modulus of the plate material.

The bending moments and twisting moments are:

$$M_{xx} = \int_{-h/2}^{h/2} \frac{Ez^2}{1-\mu^2}\left(\frac{\partial^2 w}{\partial x^2} + \mu\frac{\partial^2 w}{\partial y^2}\right)dz + \int_{-h/2}^{h/2} \frac{Ezf(z)}{1-\mu^2}\left(\frac{\partial^2 w_s}{\partial x^2} + \mu\frac{\partial^2 w_s}{\partial y^2}\right)dz \quad (21)$$

$$M_{xx} = -D\left(\frac{\partial^2 w}{\partial x^2} + \mu\frac{\partial^2 w}{\partial y^2}\right) + \frac{EI_3}{1-\mu^2}\left(\frac{\partial^2 w_s}{\partial x^2} + \mu\frac{\partial^2 w_s}{\partial y^2}\right) \quad (22)$$

$$M_{yy} = -D\left(\frac{\partial^2 w}{\partial y^2} + \mu\frac{\partial^2 w}{\partial x^2}\right) + \frac{EI_3}{1-\mu^2}\left(\frac{\partial^2 w_s}{\partial y^2} + \mu\frac{\partial^2 w_s}{\partial x^2}\right) \quad (23)$$

$$M_{xy} = -2G\int_{-h/2}^{h/2} z^2 dz\frac{\partial^2 w}{\partial x\partial y} + 2G\int_{-h/2}^{h/2} zf(z)dz\frac{\partial^2 w_s}{\partial x\partial y} \quad (24)$$

Shear force resultants are:

$$Q_x = \frac{2Gh}{\pi}\frac{\partial w_s}{\partial x} \quad (25)$$

$$Q_y = \frac{2Gh}{\pi}\frac{\partial w_s}{\partial y} \quad (26)$$

3. Ritz Variational Methodology

The Ritz variational method is based on the minimization of the total potential energy functional Π of the thick plate buckling problem. The total potential energy functional Π is the sum of the strain energy U of the thick plate and the potential energy V of the applied loads.

The in-plane forces, N_{xx}, N_{yy}, N_{xy} are:

$$N_{xx} = \int_{-h/2}^{h/2} \sigma_{xx}dz$$
$$N_{yy} = \int_{-h/2}^{h/2} \sigma_{yy}dz$$
$$N_{xy} = \int_{-h/2}^{h/2} \tau_{xy}dz \quad (27)$$
$$N_{yx} = \int_{-h/2}^{h/2} \tau_{yx}dz$$

N_{xx}, N_{yy} are in-plane normal forces, N_{xy} and N_{yx} are in-plane shear forces.

Thus $\Pi = U + V$ (28)

where

$$U = \frac{1}{2}\iiint_{R^3}(\sigma_{xx}\varepsilon_{xx} + \sigma_{yy}\varepsilon_{yy} + \sigma_{zz}\varepsilon_{zz} + \tau_{xy}\gamma_{xy} + \tau_{xz}\gamma_{xz} + \tau_{yz}\gamma_{yz})dxdydz \quad (29)$$

R^3 is the three-dimensional (3D) region (domain) of the plate.

$$V = -\frac{1}{2}\iint_{R^2}\left(N_{xx}\left(\frac{\partial w}{\partial x}\right)^2 + 2N_{xy}\left(\frac{\partial w}{\partial x}\right)\left(\frac{\partial w}{\partial y}\right) + N_{yy}\left(\frac{\partial w}{\partial y}\right)^2\right)dA \quad (30)$$

Simplifying,

$$U = \frac{1}{2}\iiint_{R^3}\left\{\frac{E}{1-\mu^2}(\varepsilon_{xx} + \mu\varepsilon_{yy})\varepsilon_{xx} + \frac{E}{1-\mu^2}(\varepsilon_{yy} + \mu\varepsilon_{xx})\varepsilon_{yy} + G\gamma_{xy}^2 + G\gamma_{xz}^2 + G\gamma_{yz}^2)\right\}dxdydz \quad (31)$$

$$U = \frac{1}{2}\iiint_{R^3}\left\{\frac{E}{1-\mu^2}(\varepsilon_{xx}^2 + \varepsilon_{yy}^2 + 2\mu\varepsilon_{xx}\varepsilon_{yy}) + G(\gamma_{xy}^2) + G(\gamma_{xz}^2 + \gamma_{yz}^2)\right\}dxdydz \quad (32)$$

$$U = \frac{E}{2(1-\mu^2)}\iiint_{R^3}(\varepsilon_{xx}^2 + \varepsilon_{yy}^2 + 2\mu\varepsilon_{xx}\varepsilon_{yy})dxdydz + \frac{G}{2}\iiint_{R^3}\gamma_{xy}^2 + \gamma_{xz}^2 + \gamma_{yz}^2)dxdydz \quad (33)$$

$$U = \frac{E}{2(1-\mu^2)}\iiint_{R^3}\left\{\left(-z\frac{\partial^2 w}{\partial x^2} + f(z)\frac{\partial^2 w_s}{\partial x^2}\right)^2 + \left(-z\frac{\partial^2 w}{\partial y^2} + f(z)\frac{\partial^2 w_s}{\partial y^2}\right)^2 + 2\mu\left(-z\frac{\partial^2 w}{\partial x^2} + f(z)\frac{\partial^2 w_s}{\partial x^2}\right)\left(-z\frac{\partial^2 w}{\partial y^2} + f(z)\frac{\partial^2 w_s}{\partial y^2}\right)\right\}dxdydz + \frac{G}{2}\iiint_{R^3}\left\{\left(-2z\frac{\partial^2 w}{\partial x\partial y} + 2f(z)\frac{\partial^2 w_s}{\partial x\partial y}\right)^2 + \left(f'(z)\frac{\partial w_s}{\partial x}\right)^2 + \left(f'(z)\frac{\partial w_s}{\partial y}\right)^2\right\}dxdydz \quad (34)$$

$$U=\frac{E}{2(1-\mu^2)}\iiint_{R^3}\left\{z^2\left(\frac{\partial^2 w}{\partial x^2}\right)^2+(f(z))^2\left(\frac{\partial^2 w_s}{\partial x^2}\right)^2-2zf(z)\frac{\partial^2 w}{\partial x^2}\frac{\partial^2 w_s}{\partial x^2}\right\}+\left\{z^2\left(\frac{\partial^2 w}{\partial y^2}\right)^2+(f(z))^2\left(\frac{\partial^2 w_s}{\partial y^2}\right)^2-2zf(z)\frac{\partial^2 w}{\partial y^2}\frac{\partial^2 w_s}{\partial y^2}\right\}+2\mu\left(z^2\frac{\partial^2 w}{\partial x^2}\frac{\partial^2 w}{\partial y^2}-zf(z)\frac{\partial^2 w_s}{\partial x^2}\frac{\partial^2 w}{\partial y^2}-zf(z)\frac{\partial^2 w}{\partial x^2}\frac{\partial^2 w_s}{\partial y^2}+(f(z))^2\frac{\partial^2 w_s}{\partial x^2}\frac{\partial^2 w_s}{\partial y^2}\right)dxdydz+\frac{G}{2}\iiint_{R^3}\left[4z^2\left(\frac{\partial^2 w}{\partial x\partial y}\right)^2+4(f(z))^2\left(\frac{\partial^2 w_s}{\partial x\partial y}\right)^2+8zf(z)\frac{\partial^2 w}{\partial x\partial y}\frac{\partial^2 w_s}{\partial x\partial y}+(f'(z))^2\left(\frac{\partial w_s}{\partial x}\right)^2+(f'(z))^2\left(\frac{\partial w_s}{\partial y}\right)^2\right]dxdydz \qquad (35)$$

$$U=\frac{E}{2(1-\mu^2)}\iint_{R^2}\left\{I_1\left(\frac{\partial^2 w}{\partial x^2}\right)^2+I_2\left(\frac{\partial^2 w_s}{\partial x^2}\right)^2-2I_3\frac{\partial^2 w}{\partial x^2}\frac{\partial^2 w_s}{\partial x^2}+I_1\left(\frac{\partial^2 w_s}{\partial y^2}\right)^2+I_2\left(\frac{\partial^2 w_s}{\partial y^2}\right)^2-2I_3\frac{\partial^2 w}{\partial y^2}\frac{\partial^2 w_s}{\partial y^2}+2\mu\left(I_1\frac{\partial^2 w}{\partial x^2}\frac{\partial^2 w}{\partial y^2}-I_3\frac{\partial^2 w_s}{\partial x^2}\frac{\partial^2 w}{\partial y^2}-I_3\frac{\partial^2 w_s}{\partial y^2}\frac{\partial^2 w}{\partial x^2}+I_2\frac{\partial^2 w_s}{\partial x^2}\frac{\partial^2 w_s}{\partial y^2}\right)\right\}dA+\frac{G}{2}\iint_{R^2}\left[4I_1\left(\frac{\partial^2 w}{\partial x\partial y}\right)^2+4I_2\left(\frac{\partial^2 w_s}{\partial x\partial y}\right)^2+8I_3\frac{\partial^2 w}{\partial x\partial y}\frac{\partial^2 w_s}{\partial x\partial y}+I_4\left(\frac{\partial w_s}{\partial x}\right)^2+I_4\left(\frac{\partial w_s}{\partial y}\right)^2\right]dA \qquad (36)$$

wherein,

$$I_1=\int_{-h/2}^{h/2}z^2dz;\quad I_2=\frac{h^3}{12}$$

$$I_2=\int_{-h/2}^{h/2}(f(z))^2\,dz;\quad I_2=\int_{-h/2}^{h/2}\frac{h^2}{\pi^2}\sin^2\left(\frac{\pi z}{h}\right)dz$$

$$I_2=\frac{h^3}{2\pi^2}$$

$$I_3=\int_{-h/2}^{h/2}zf(z)dz;\quad I_3=\int_{-h/2}^{h/2}\frac{h}{\pi}z\sin\frac{\pi z}{h}\,dz$$

$$I_3=\frac{2h^3}{\pi^3}$$

$$I_4=\int_{-h/2}^{h/2}(f'(z))^2\,dz;\ I_4=\int_{-h/2}^{h/2}\cos^2\left(\frac{\pi z}{h}\right)dz$$

$$I_4=\frac{h}{2} \qquad (37)$$

$$I_2=\frac{6I_1}{\pi^2}$$

$$I_3=\frac{24I_1}{\pi^3} \qquad (38)$$

$$I_4=\frac{6I_1}{h^2}$$

$$G=\frac{E}{2(1+\mu)};\quad \frac{G}{2}=\frac{E}{4(1+\mu)}$$

$$V_1=-\frac{1}{2}\iint_{R^2}N_{xx}\left(\frac{\partial w}{\partial x}\right)^2dxdy \qquad (39)$$

$$V_2=-\frac{1}{2}\iint_{R^2}N_{yy}\left(\frac{\partial w}{\partial y}\right)^2dxdy \qquad (40)$$

$$V_3=-\frac{1}{2}\iint_{R^2}\left(N_{xx}\left(\frac{\partial w}{\partial x}\right)^2+N_{yy}\left(\frac{\partial w}{\partial y}\right)^2\right)dxdy \qquad \ldots(41a)$$

$$V_3=-\frac{1}{2}N_0\iint_{R^2}\left(\left(\frac{\partial w}{\partial x}\right)^2+\left(\frac{\partial w}{\partial y}\right)^2\right)dxdy \qquad (41b)$$

$$\delta V_3=N_0\iint_{R^2}\nabla^2 w\,dxdy \qquad (42a)$$

$$\delta V_3=N_0\iint_{R^2}\nabla^2(w_b+w_s)\,dxdy \qquad (42b)$$

$$\delta V_3=N_0\iint_{R^2}(\nabla^2 w_b+\nabla^2 w_s)\,dxdy \qquad (42c)$$

Then, the expression for Π is:

$$\Pi=\frac{E}{2(1-\mu^2)}\iint_{R^2}\left\{I_1\left(\frac{\partial^2 w_b}{\partial x^2}+\frac{\partial^2 w_s}{\partial x^2}\right)^2+\right.$$

$$I_2\left(\frac{\partial^2 w_s}{\partial x^2}\right)^2 - 2I_3\left(\frac{\partial^2 w_s}{\partial x^2}\right)\left(\frac{\partial^2 w_b}{\partial x^2}+\frac{\partial^2 w_s}{\partial x^2}\right)+$$
$$I_1\left(\frac{\partial^2 w_b}{\partial y^2}+\frac{\partial^2 w_s}{\partial y^2}\right)^2 + I_2\left(\frac{\partial^2 w_s}{\partial y^2}\right)^2 -$$
$$2I_3\frac{\partial^2 w_s}{\partial y^2}\left(\frac{\partial^2 w_b}{\partial y^2}+\frac{\partial^2 w_s}{\partial y^2}\right)+2\mu\left(I_1\left(\frac{\partial^2 w_b}{\partial x^2}+\right.\right.$$
$$\left.\frac{\partial^2 w_s}{\partial x^2}\right)\left(\frac{\partial^2 w_b}{\partial y^2}+\frac{\partial^2 w_s}{\partial y^2}\right)-I_3\frac{\partial^2 w_s}{\partial x^2}\left(\frac{\partial^2 w_b}{\partial y^2}+\frac{\partial^2 w_s}{\partial y^2}\right)-$$
$$\left.I_3\frac{\partial^2 w_s}{\partial y^2}\left(\frac{\partial^2 w_b}{\partial x^2}+\frac{\partial^2 w_s}{\partial x^2}\right)+I_2\frac{\partial^2 w_s}{\partial x^2}\frac{\partial^2 w_s}{\partial y^2}\right)\Bigg\}dA+$$
$$\frac{G}{2}\iint_{R^2}\Bigg[4I_1\left(\frac{\partial^2(w_b+w_s)}{\partial x\partial y}\right)^2+4I_2\left(\frac{\partial^2 w_s}{\partial x\partial y}\right)^2+$$
$$8I_3\frac{\partial^2 w_s}{\partial x\partial y}\left(\frac{\partial^2(w_b+w_s)}{\partial x\partial y}\right)+I_4\left(\frac{\partial w_s}{\partial x}\right)^2+$$
$$I_4\left(\left(\frac{\partial w_b}{\partial y}\right)^2+\left(\frac{\partial w_s}{\partial y}\right)^2\right)\Bigg]dA-V \qquad (43)$$

Simplifying,

$$\Pi = D_1\iint_{R^2}\left(\left(\frac{\partial^2 w_b}{\partial x^2}\right)^2+2\frac{\partial^2 w_b}{\partial x^2}\frac{\partial^2 w_s}{\partial x^2}+\right.$$
$$\left.\left(\frac{\partial^2 w_s}{\partial x^2}\right)^2\right)dxdy + D_2\iint_{R^2}\left(\frac{\partial^2 w_s}{\partial x^2}\right)^2 dxdy -$$
$$2D_3\iint_{R^2}\left\{\frac{\partial^2 w_s}{\partial x^2}\frac{\partial^2 w_b}{\partial x^2}+\left(\frac{\partial^2 w_s}{\partial x^2}\right)^2\right\}dxdy+$$
$$D_1\iint_{R^2}\left(\left(\frac{\partial^2 w_b}{\partial y^2}\right)^2+2\frac{\partial^2 w_b}{\partial y^2}\frac{\partial^2 w_s}{\partial y^2}+\left(\frac{\partial^2 w_s}{\partial y^2}\right)^2\right)dxdy+$$
$$D_2\iint_{R^2}\left(\frac{\partial^2 w_s}{\partial y^2}\right)^2 dxdy - 2D_3\iint_{R^2}\left\{\frac{\partial^2 w_s}{\partial y^2}\frac{\partial^2 w_b}{\partial y^2}+\right.$$
$$\left.\left(\frac{\partial^2 w_s}{\partial y^2}\right)^2\right\}dxdy + 2\mu D_1\iint_{R^2}\left(\frac{\partial^2 w_b}{\partial x^2}\frac{\partial^2 w_b}{\partial y^2}+\right.$$
$$\frac{\partial^2 w_s}{\partial x^2}\frac{\partial^2 w_b}{\partial y^2}+\frac{\partial^2 w_b}{\partial x^2}\frac{\partial^2 w_s}{\partial y^2}+\frac{\partial^2 w_s}{\partial x^2}\frac{\partial^2 w_s}{\partial y^2}\Bigg)dxdy -$$
$$2\mu D_3\iint_{R^2}\left\{\left(\frac{\partial^2 w_s}{\partial x^2}\frac{\partial^2 w_b}{\partial y^2}+\frac{\partial^2 w_s}{\partial x^2}\frac{\partial^2 w_s}{\partial y^2}\right)+\right.$$
$$\left.\left(\frac{\partial^2 w_s}{\partial y^2}\frac{\partial^2 w_b}{\partial x^2}+\frac{\partial^2 w_s}{\partial y^2}\frac{\partial^2 w_s}{\partial x^2}\right)\right\}dxdy +$$
$$2\mu D_2\iint_{R^2}\left(\frac{\partial^2 w_s}{\partial x^2}\frac{\partial^2 w_s}{\partial y^2}\right)dxdy + \frac{D_1(1-\mu)}{2}\times$$
$$4\iint_{R^2}\left(\left(\frac{\partial^2 w_b}{\partial x\partial y}\right)^2+\left(\frac{\partial^2 w_s}{\partial x\partial y}\right)^2\right)dxdy +$$
$$\frac{D_2(1-\mu)}{2}\cdot 4\iint_{R^2}\left(\frac{\partial^2 w_s}{\partial x\partial y}\right)^2 dxdy + \frac{D_3(1-\mu)}{2}\times$$
$$8\iint_{R^2}\left(\frac{\partial^2 w_s}{\partial x\partial y}\frac{\partial^2 w_b}{\partial x\partial y}+\left(\frac{\partial^2 w_s}{\partial x\partial y}\right)^2\right)dxdy +$$
$$\frac{Gh}{4}\iint_{R^2}\left\{\left(\frac{\partial w_s}{\partial x}\right)^2+\left(\frac{\partial w_b}{\partial y}\right)^2+2\frac{\partial w_b}{\partial y}\frac{\partial w_s}{\partial y}+\right.$$
$$\left.\left(\frac{\partial w_s}{\partial y}\right)^2\right\}dxdy - V \qquad (44)$$

where

$$\nabla^2 w_s = \left(\frac{\partial^2}{\partial x^2}+\frac{\partial^2}{\partial y^2}\right)w_s = \frac{\partial^2 w_s}{\partial x^2}+\frac{\partial^2 w_s}{\partial y^2}$$
$$\nabla^2 w_b = \left(\frac{\partial^2}{\partial x^2}+\frac{\partial^2}{\partial y^2}\right)w_b = \frac{\partial^2 w_b}{\partial x^2}+\frac{\partial^2 w_b}{\partial y^2} \qquad (45)$$

$$D_1 = \frac{EI_1}{2(1-\mu^2)}$$
$$D_2 = \frac{EI_2}{2(1-\mu^2)}$$
$$D_2 = D_1\cdot\frac{6}{\pi^2}$$
$$D_3 = \frac{EI_3}{2(1-\mu^2)}$$
$$D_3 = D_1\cdot\frac{24}{\pi^3}$$
$$G = \frac{E}{2(1+\mu)}$$
$$\frac{G}{2} = \frac{E(1-\mu)}{4(1-\mu^2)}; \qquad \frac{G}{E} = \frac{1}{2(1+\mu)}$$
$$\frac{G}{2}I_1 = \frac{E(1-\mu)}{4(1-\mu^2)}I_1$$
$$\frac{G}{2}I_1 = D_1\left(\frac{1-\mu}{2}\right)$$

$$\frac{G}{2} I_2 = \frac{E(1-\mu)}{4(1-\mu^2)} I_2$$

$$\frac{G}{2} I_2 = D_1 \frac{6}{\pi^2}\left(\frac{1-\mu}{2}\right)$$

$$\frac{G}{2} I_3 = \frac{D_3(1-\mu)}{2}, \quad \frac{GI_4}{2} = \frac{Gh}{4}$$

For extremum of $\prod$,

$$\delta \prod = 0 \qquad (46)$$

where δ is the variational operator.

Integrating Equation (44) by parts, and setting the coefficients of δw_b and δw_s equal to zero, the Euler-Lagrange equations of stability become:

$$D\nabla^4 w_b + D\left(1+\frac{24}{\pi^3}\right)\nabla^4 w_s + N_{xx}\frac{\partial^2 w_b}{\partial x^2} + 2N_{xy}\frac{\partial^2 w_b}{\partial x \partial y} + N_{yy}\frac{\partial^2 w_b}{\partial y^2} + N_{xx}\frac{\partial^2 w_s}{\partial x^2} + 2N_{xy}\frac{\partial^2 w_s}{\partial x \partial y} + N_{yy}\frac{\partial^2 w_s}{\partial y^2} = 0 \qquad (47)$$

$$D\left(1-\frac{24}{\pi^3}\right)\nabla^4 w_b + D\left(1+\frac{6}{\pi^2}-\frac{48}{\pi^3}\right)\nabla^4 w_s - \frac{Eh}{4(1+\mu)}\nabla^2 w_s + N_{xx}\frac{\partial^2 w_b}{\partial x^2} + 2N_{xy}\frac{\partial^2 w_b}{\partial x \partial y} + N_{yy}\frac{\partial^2 w_b}{\partial y^2} + N_{xx}\frac{\partial^2 w_s}{\partial x^2} + 2N_{xy}\frac{\partial^2 w_s}{\partial x \partial y} + N_{yy}\frac{\partial^2 w_s}{\partial y^2} = 0 \qquad (48)$$

where $D = \frac{Eh^3}{12(1-\mu^2)}$ (49)

D is the modulus of flexural rigidity of the plate material.

For uniaxial loading in the x-direction, $N_{yy} = 0$, $N_{xy} = 0$, the governing equations are:

$$D\nabla^4 w_b + D\left(1-\frac{24}{\pi^3}\right)\nabla^4 w_s + N_{xx}\frac{\partial^2 w_b}{\partial x^2} + N_{xx}\frac{\partial^2 w_s}{\partial x^2} = 0 \qquad (50)$$

$$D\left(1-\frac{24}{\pi^3}\right)\nabla^4 w_b + D\left(1+\frac{6}{\pi^2}-\frac{48}{\pi^3}\right)\nabla^4 w_s - \frac{Eh}{4(1+\mu)}\nabla^2 w_s + N_{xx}\frac{\partial^2 w_b}{\partial x^2} + N_{xx}\frac{\partial^2 w_s}{\partial x^2} = 0 \qquad \ldots(51)$$

For uniaxial loading in the y-direction, $N_{xx} = 0$, $N_{xy} = 0$, the governing equations are:

$$D\nabla^4 w_b + D\left(1-\frac{24}{\pi^3}\right)\nabla^4 w_s + N_{yy}\frac{\partial^2 w_b}{\partial y^2} + N_{yy}\frac{\partial^2 w_s}{\partial y^2} = 0 \qquad (52)$$

$$D\left(1-\frac{24}{\pi^3}\right)\nabla^4 w_b + D\left(1+\frac{6}{\pi^2}-\frac{48}{\pi^3}\right)\nabla^4 w_s - \frac{Eh}{4(1+\mu)}\nabla^2 w_s + N_{yy}\frac{\partial^2 w_b}{\partial y^2} + N_{yy}\frac{\partial^2 w_s}{\partial y^2} = 0 \qquad \ldots(53)$$

For biaxial loading in the x and y directions, $N_{xy} = 0$, the governing equations are:

$$D\nabla^4 w_b + D\left(1-\frac{24}{\pi^3}\right)\nabla^4 w_s + N_{xx}\frac{\partial^2 w_b}{\partial x^2} + N_{yy}\frac{\partial^2 w_b}{\partial y^2} + N_{xx}\frac{\partial^2 w_s}{\partial x^2} + N_{yy}\frac{\partial^2 w_s}{\partial y^2} = 0 \qquad (54)$$

$$D\left(1-\frac{24}{\pi^3}\right)\nabla^4 w_b + D\left(1+\frac{6}{\pi^2}-\frac{48}{\pi^3}\right)\nabla^4 w_s - \frac{Eh}{4(1+\mu)}\nabla^2 w_s + N_{xx}\frac{\partial^2 w_b}{\partial x^2} + N_{yy}\frac{\partial^2 w_b}{\partial y^2} + N_{xx}\frac{\partial^2 w_s}{\partial x^2} + N_{yy}\frac{\partial^2 w_s}{\partial y^2} = 0 \qquad (55)$$

3. Methodology

3.1 The Galerkin Variational Functional (GVF)

For simply supported boundaries, the boundary conditions are:

$$\begin{aligned} &w_b(0,0) = 0; \quad w_b''(0,0) = 0 \\ &w_b(a,0) = 0; \quad w_b''(a,0) = 0 \\ &w_s(0,0) = 0; \quad w_s''(0,0) = 0 \\ &w_s(0,b) = 0; \quad w_s''(0,b) = 0 \end{aligned} \qquad (56)$$

Hence the displacement functions that satisfy the BCs are:

$$w_b(x,y) = w_{b_{mn}} \sin\left(\frac{m\pi x}{a}\right)\sin\left(\frac{n\pi y}{b}\right) \qquad (57)$$

$$w_s(x,y) = w_{s_{mn}} \sin\left(\frac{m\pi x}{a}\right)\sin\left(\frac{n\pi y}{b}\right) \qquad (58)$$

where m, n = 1, 2, 3, 4, …; $w_{b_{mn}}$ is the buckling bending displacement component amplitude for the mn buckling mode; $w_{s_{mn}}$

is the buckling shear displacement amplitude component for the *mn* buckling mode.

$$w_b(x,y) = w_{b_{mn}} \sin(\alpha_m x)\sin(\beta_n y)$$
$$w_s(x,y) = w_{s_{mn}} \sin(\alpha_m x)\sin(\beta_n y) \quad (59)$$

where $\alpha_m = m\pi/a, \quad \beta_n = n\pi/b \quad (60)$

The GVF for the biaxially compressed thick plate problem shown in Figure 2(iii) is the system of equations:

$$\int_0^b\int_0^a \Big\{ D\nabla^4 w_{b_{mn}} \sin(\alpha_m x)\sin(\beta_n y) +$$
$$D\left(1-\frac{24}{\pi^3}\right)\nabla^4 w_{s_{mn}} \sin(\alpha_m x)\sin(\beta_n y) +$$
$$N_{xx}\frac{\partial^2}{\partial x^2} w_{b_{mn}} \sin(\alpha_m x)\sin(\beta_n y) +$$
$$N_{xx}\frac{\partial^2}{\partial x^2} w_{s_{mn}} \sin(\alpha_m x)\sin(\beta_n y) +$$
$$N_{yy}\frac{\partial^2}{\partial y^2} w_{b_{mn}} \sin(\alpha_m x)\sin(\beta_n y) +$$
$$N_{yy}\frac{\partial^2}{\partial y^2} w_{s_{mn}} \sin(\alpha_m x)\sin(\beta_n y)\Big\} \times$$
$$\sin(\bar{\alpha}_m x)\sin(\bar{\beta}_n y)dxdy = 0 \quad (61)$$

where $\bar{\alpha}_m = \frac{\bar{m}\pi}{a}, \quad \bar{\beta}_n = \frac{\bar{n}\pi}{b} \quad (62)$

where $\bar{m}, \bar{n} = 1, 2, 3, 4, \ldots$

$$\int_0^b\int_0^a \Big\{ D\left(1-\frac{24}{\pi^3}\right)\nabla^4 w_{b_{mn}} \sin(\alpha_m x)\sin(\beta_n y) +$$
$$D\left(1+\frac{6}{\pi^2}-\frac{48}{\pi^3}\right)\nabla^4 w_{s_{mn}} \sin(\alpha_m x)\sin(\beta_n y) -$$
$$\frac{Eh}{4(1+\mu)}\nabla^2 w_{s_{mn}} \sin(\alpha_m x)\sin(\beta_n y) +$$
$$N_{xx}\frac{\partial^2}{\partial x^2} w_{b_{mn}} \sin(\alpha_m x)\sin(\beta_n y) +$$
$$N_{xx}\frac{\partial^2}{\partial x^2} w_{s_{mn}} \sin(\alpha_m x)\sin(\beta_n y) +$$
$$N_{yy}\frac{\partial^2}{\partial y^2} w_{b_{mn}} \sin(\alpha_m x)\sin(\beta_n y) +$$
$$N_{yy}\frac{\partial^2}{\partial y^2} w_{s_{mn}} \sin(\alpha_m x)\sin(\beta_n y)\Big\} \times$$
$$\sin(\bar{\alpha}_m x)\sin(\bar{\beta}_n y)dxdy = 0 \quad (63)$$

Simplifying,

$$\nabla^4 w_{b_{mn}} \sin(\alpha_m x)\sin(\beta_n y) = w_{b_{mn}}(\alpha_m^4 + 2\alpha_m^2\beta_n^2 + \beta_n^4)\sin(\alpha_m x)\sin(\beta_n y) \quad (64)$$

$$\nabla^4 w_{s_{mn}} \sin(\alpha_m x)\sin(\beta_n y) = w_{s_{mn}}(\alpha_m^4 + 2\alpha_m^2\beta_n^2 + \beta_n^4)\sin(\alpha_m x)\sin(\beta_n y) \quad (65)$$

$$\frac{\partial^2}{\partial x^2} w_{b_{mn}} \sin(\alpha_m x)\sin(\beta_n y) = -w_{b_{mn}}\alpha_m^2 \sin(\alpha_m x)\sin(\beta_n y) \quad (66)$$

$$\frac{\partial^2}{\partial x^2} w_{s_{mn}} \sin(\alpha_m x)\sin(\beta_n y) = -w_{s_{mn}}\alpha_m^2 \sin(\alpha_m x)\sin(\beta_n y) \quad (67)$$

$$\frac{\partial^2}{\partial y^2} w_{b_{mn}} \sin(\alpha_m x)\sin(\beta_n y) = -w_{b_{mn}}\beta_n^2 \sin(\alpha_m x)\sin(\beta_n y) \quad (68)$$

$$\frac{\partial^2}{\partial y^2} w_{s_{mn}} \sin(\alpha_m x)\sin(\beta_n y) = -w_{s_{mn}}\beta_n^2 \sin(\alpha_m x)\sin(\beta_n y) \quad (69)$$

$$\nabla^2 w_{s_{mn}} \sin(\alpha_m x)\sin(\beta_n y) = -(\alpha_m^2 + \beta_n^2) w_{s_{mn}} \sin(\alpha_m x)\sin(\beta_n y) \quad (70)$$

Simplifying Equation (61) gives:

$$\Big\{ Dw_{b_{mn}}(\alpha_m^4 + 2\alpha_m^2\beta_n^2 + \beta_n^4) +$$
$$D\left(1-\frac{24}{\pi^3}\right) w_{s_{mn}}(\alpha_m^4 + 2\alpha_m^2\beta_n^2 + \beta_n^4) - N_{xx}\alpha_m^2 w_{bmn} -$$
$$N_{xx}\alpha_m^2 w_{s_{mn}} - N_{yy}\beta_n^2 w_{b_{mn}} - N_{yy}\beta_n^2 w_{s_{mn}}\Big\} \times$$
$$\int_0^b\int_0^a \left(\sin(\alpha_m x)\sin(\beta_n y)\sin(\bar{\alpha}_m x)\sin(\bar{\beta}_n y)\right)dxdy = 0 \quad \ldots(71)$$

It is observed that $\sin\alpha_m x, \sin\beta_n y$ are orthogonal functions.

Hence,

$$\int_0^b\int_0^a \sin(\alpha_m x)\sin(\beta_n y)\sin(\bar{\alpha}_m x)\sin(\bar{\beta}_n y)dxdy = \int_0^b\int_0^a \sin^2(\alpha_m x)\sin^2(\beta_n y)dxdy \quad (72)$$

and zero if $m \neq \bar{m}, n \neq \bar{n}$

Simplifying Equation (63) gives:

$$\Big\{ D\left(1-\frac{24}{\pi^3}\right) w_{b_{mn}}(\alpha_m^4 + 2\alpha_m^2\beta_n^2 + \beta_n^4) +$$

$$D\left(1+\frac{6}{\pi^2}-\frac{48}{\pi^3}\right)w_{s_{mn}}(\alpha_m^4+2\alpha_m^2\beta_n^2+\beta_n^4)+$$
$$\frac{Eh}{4(1+\mu)}(\alpha_m^2+\beta_n^2)w_{s_{mn}}-N_{xx}\alpha_m^2 w_{bmn}-$$
$$N_{xx}\alpha_m^2 w_{s_{mn}}-N_{yy}\beta_n^2 w_{b_{mn}}-N_{yy}\beta_n^2 w_{s_{mn}}\Big\}\times$$

$$\int_0^b\int_0^a\left(\sin(\alpha_m x)\sin(\beta_n y)\sin(\bar{\alpha}_m x)\sin(\bar{\beta}_n y)\right)dxdy=0 \quad \ldots(73)$$

Let,

$$I_{mn}=\int_0^b\int_0^a\left(\sin^2(\alpha_m x)\sin^2(\beta_n y)\right)dxdy \quad (74)$$

Simplifying Equations (71) and (73) further give:

$$\Big\{Dw_{b_{mn}}(\alpha_m^4+2\alpha_m^2\beta_n^2+\beta_n^4)+$$
$$\left(1-\frac{24}{\pi^3}\right)w_{s_{mn}}D(\alpha_m^4+2\alpha_m^2\beta_n^2+\beta_n^4)-$$
$$N_{xx}\alpha_m^2 w_{bmn}-N_{xx}\alpha_m^2 w_{s_{mn}}-N_{yy}\beta_n^2 w_{b_{mn}}-$$
$$N_{yy}\beta_n^2 w_{s_{mn}}\Big\}I_{mn}=0 \quad (75)$$

$$\Big\{\left(1-\frac{24}{\pi^3}\right)w_{b_{mn}}D(\alpha_m^4+2\alpha_m^2\beta_n^2+\beta_n^4)+$$
$$\left(1+\frac{6}{\pi^2}-\frac{48}{\pi^3}\right)w_{s_{mn}}D(\alpha_m^4+2\alpha_m^2\beta_n^2+\beta_n^4)+$$
$$\frac{Eh}{4(1+\mu)}(\alpha_m^2+\beta_n^2)w_{s_{mn}}-N_{xx}\alpha_m^2 w_{b_{mn}}-$$
$$N_{xx}\alpha_m^2 w_{s_{mn}}-N_{yy}\beta_n^2 w_{b_{mn}}-N_{yy}\beta_n^2 w_{s_{mn}}\Big\}I_{mn}=0$$
$$\ldots(76)$$

Let,

$$N_{xx}=k_1N_0$$
$$N_{yy}=k_2N_0 \quad (77)$$

where N_0 is a constant (uniform) compressive load, then, for non-trivial solutions, $I_{mn}\neq 0$, and

$$D(\alpha_m^4+2\alpha_m^2\beta_n^2+\beta_n^4)w_{b_{mn}}-k_1N_0\alpha_m^2 w_{b_{mn}}-$$
$$k_2N_0\beta_n^2 w_{b_{mn}}+D\left(1-\frac{24}{\pi^3}\right)(\alpha_m^4+2\alpha_m^2\beta_n^2+$$
$$\beta_n^4)w_{s_{mn}}-k_1N_0\alpha_m^2 w_{s_{mn}}-k_2N_0 w_{s_{mn}}=0 \quad \ldots(78)$$

$$\left(1-\frac{24}{\pi^3}\right)(\alpha_m^4+2\alpha_m^2\beta_n^2+\beta_n^4)Dw_{b_{mn}}-$$
$$k_1N_0\alpha_m^2 w_{b_{mn}}-k_2N_0\beta_n^2 w_{b_{mn}}+$$
$$D\left(1+\frac{6}{\pi^2}-\frac{24}{\pi^3}\right)(\alpha_m^4+2\alpha_m^2\beta_n^2+\beta_n^4)w_{s_{mn}}+$$
$$\frac{Eh}{4(1+\mu)}(\alpha_m^2+\beta_n^2)w_{s_{mn}}-$$
$$k_1N_0\alpha_m^2 w_{s_{mn}}-k_2N_0\beta_n^2 w_{s_{mn}}=0 \quad (79)$$

In matrix format,

$$\begin{pmatrix}s_{11}&s_{12}\\s_{21}&s_{22}\end{pmatrix}\begin{pmatrix}w_{b_{mn}}\\w_{s_{mn}}\end{pmatrix}-N_0\begin{pmatrix}\bar{s}_{11}&\bar{s}_{12}\\\bar{s}_{21}&\bar{s}_{22}\end{pmatrix}\begin{pmatrix}w_{b_{mn}}\\w_{s_{mn}}\end{pmatrix}=\begin{pmatrix}0\\0\end{pmatrix}$$
$$\ldots(80)$$

where s_{ij} are elastic stiffness coefficients (parameters)

$\bar{s}_{ij}$ are geometric stiffness coefficients (parameters)

$$s_{11}=D(\alpha_m^4+2\alpha_m^2\beta_n^2+\beta_n^4)$$
$$s_{21}=s_{12}=D\left(1-\frac{24}{\pi^3}\right)(\alpha_m^4+2\alpha_m^2\beta_n^2+\beta_n^4)$$
$$s_{22}=D\left(1+\frac{6}{\pi^2}-\frac{48}{\pi^3}\right)(\alpha_m^4+$$
$$2\alpha_m^2\beta_n^2+\beta_n^4)+\frac{Eh}{4(1+\mu)}(\alpha_m^2+\beta_n^2) \quad (81)$$

$$\bar{s}_{11}=k_1\alpha_m^2+k_2\beta_n^2$$
$$\bar{s}_{12}=\bar{s}_{21}=\bar{s}_{22}=\bar{s}_{11}$$

Hence,

$$\left\{\begin{pmatrix}s_{11}&s_{12}\\s_{21}&s_{22}\end{pmatrix}-N_0\begin{pmatrix}\bar{s}_{11}&\bar{s}_{12}\\\bar{s}_{21}&\bar{s}_{22}\end{pmatrix}\right\}\begin{pmatrix}w_{b_{mn}}\\w_{s_{mn}}\end{pmatrix}=\begin{pmatrix}0\\0\end{pmatrix}$$
$$\ldots(82)$$

Or,

$$\begin{pmatrix}s_{11}-N_0\bar{s}_{11}&s_{12}-N_0\bar{s}_{12}\\s_{21}-N_0\bar{s}_{12}&s_{22}-N_0\bar{s}_{22}\end{pmatrix}\begin{pmatrix}w_{b_{mn}}\\w_{s_{mn}}\end{pmatrix}=\begin{pmatrix}0\\0\end{pmatrix}$$
$$\ldots(83)$$

For non-trivial solutions,

$$\begin{vmatrix}s_{11}-N_0\bar{s}_{11}&s_{12}-N_0\bar{s}_{12}\\s_{21}-N_0\bar{s}_{21}&s_{22}-N_0\bar{s}_{22}\end{vmatrix}=0 \quad (84)$$

The characteristic buckling equation is

$$(s_{11}-N_0\bar{s}_{11})(s_{22}-N_0\bar{s}_{22})-$$
$$(s_{12}-N_0\bar{s}_{12})(s_{21}-N_0\bar{s}_{21})=0 \quad (85)$$

4. Results

A thick rectangular isotropic plate with elastic properties given by: E = 210GPa, $\mu = 0.30$ is considered. The plate is homogeneous and simply supported on all edges $x = 0$, $x = a$, $y = 0$, $y = b$. The critical buckling load N_{cr} is computed by solving for the roots of Equation (85) and presented in the dimensionless form:

$$\hat{N}_{cr} = \frac{N_0 a^2}{Eh^3};\ \frac{N_0 a^2}{12(1-\mu^2)D} = \hat{N}_{cr} \qquad (86)$$

Alternatively, $\bar{N}_{cr}$ is defined and presented in Equation (87)

$$\bar{N}_{cr} = \frac{N_0 a^2}{\pi^2 D} \qquad (87)$$

The problems considered are uniaxial buckling along the x direction, uniaxial buckling along the y direction and biaxial buckling along the x and y directions, as illustrated in Figures 2(i), 2(ii) and 2(iii).

The critical buckling load parameters are presented in dimensionless form for the case of plate subjected to uniform tensile load in the x direction and uniform compressive load in the y direction in Figure 8. The critical buckling load parameters were found for the case of plate under tensile and compressive loads when $m = 1$, $n = 2$.

The critical buckling loads N_{xxcr} for uniaxial buckling in the x direction are obtained by setting $k_2 = 0$, $k_1 = 1$ and are presented for a/h = 5, 10, 20, 50, 100 and b/a = 1, 1.5, 2, 2.5, 3, 3.5, 4 in Table 1 along with previous results. The critical buckling loads in the y direction ($N_{yy\,cr}$) are similarly obtained by setting $k_1 = 0$, $k_2 = 1$ and solving the characteristic buckling equation – Equation (85). The results for $N_{yy\,cr}$ are presented for a/h = 5, 10, 20, 50, 100 and b/a = 1, 1.5, 2, 2.5, 3, 3.5, 4 in Table 2 together with previous results. The critical buckling loads for uniform biaxial compression in the x and y directions are found by solving the characteristic buckling equation for $k_1 = k_2 = 1$ and are presented in Table 3.

The results are also presented for h/a = 0.01, 0.05, 0.1, 0.2 and b/a = 1 in terms of the dimensionless buckling parameters $\bar{N}_{cr}$ in Table 4 for uniaxial buckling in the x direction and in Table 5 for biaxial uniform buckling in both the x and y directions for h/a = 0.01, 0.05, 0.1, 0.2 and b/a = 1.

5. Discussion

This study has derived the GPDE for rectangular thick buckling using first principles variational methods. The GPDE is a system of two coupled partial differential equations. Galerkin variational method was used to obtain exact analytical and numerical solutions for simply supported rectangular thick plate subjected to uniaxial uniform compressive loads in the x and y directions respectively and biaxial uniform compressive load in both the x and y directions.

Table 1 shows the present and previous results for dimensionless critical buckling load coefficients for uniaxial uniform load in the x direction. Table 1 is graphed for square plate in Figure 3. $N_{xx\,cr}$ values are computed for a/h = 5, 10, 20, 50, 100 and for b/a = 1, 1.5, 2, 2.5, 3, 3.5, 4.

$N_{xx\,cr}$ values computed for the present study are identical with previous values by Gunjal et al (2015), Reddy (1984), Mindlin (1951), but differ significantly from the CPT results, especially when the $a/h < 100$. However, for a/h = 50 and a/h = 100, the present results and previous results by Gunjal et al (2015), Reddy (1984), Mindlin (1951), and Sayyad and Ghugal (2014) are close to CPT results.

Table 2 similarly presents results for critical uniaxial buckling loads in the y direction $N_{yy\,cr}$ for a/h = 5, 10, 20, 50, 100 and for b/a = 1, 1.5, 2, 2.5, 3, 3.5, 4. Table 2 is presented in graph form as Figure 4 for square plates. Table 2 shows that present results for $N_{yy\,cr}$ are close to results by Reddy (1984), Gunjal et al (2015), Mindlin (1951), for all values of a/h and b/a. However, the present values of $N_{yy\,cr}$ are

lower than the results by Sayyad and Ghugal (2014) for $a/h = 5$ by 2.61% for $b/a = 1$, 2% for $b/a = 1.5$, and 1.16% for $b/a = 4$. The present $N_{yy\ cr}$ values are lower than the results by Sayyad and Ghugal (2014) for $a/h = 10$ by 0.52% for $b/a = 1$ and 0.65% for $b/a = 3.5$, $b/a = 4$.

The present $N_{yy\ cr}$ results are significantly different from the CPT results for $a/h = 5, 10, 20$, but are close to the CPT results when $a/h = 50$ and $a/h = 100$. The present $N_{yy\ cr}$ results for $a/h = 5$, $b/a = 2$ is 14.1% lower than the corresponding value for CPT, illustrating how much CPT overestimates the $N_{yy\ cr}$ for thick plates and is unsafe for buckling analysis of thick plates.

Table 3 shows the non dimensional critical buckling loads for biaxially compressed thick plate buckling. Table 3 is graphed in Figure 5 as N_{cr} vs a/h for square plate and in Figure 6 as N_{cr} vs b/a for $a/h = 5$ (thick plate). The present results for N_{cr} are close to results by Gunjal et al (2015), Reddy (1984), Mindlin (1951) for all aspect ratios and for all a/h ratios, but significantly different from CPT results except for $a/h = 50$, and $a/h = 100$.

For $a/h = 5$, $b/a = 3$, N_{cr} from present study is 0.892 while CPT is 1.004 giving a different of –12.56%. This illustrates the extent that CPT overestimates the buckling loads for thick plates, rending it unsafe for thick plate design against buckling.

Table 4 presents $N_{xx\ cr}$ for uniaxial uniform compression in the x direction for square plates for $h/a = 0.01, 0.05, 0.10, 0.20$. Table 4 shows that the $N_{xx\ cr}$ values are close to previous results by Ike (2023a), Hashemi et al (2008), Thai and Choi (2013), Srinivas and Rao (1969), Reddy and Phan (1985) and Deepak et al (2021), but significantly different from CPT results by Timoshenko and Gere (1961).

Table 5 presents N_{cr} for simply supported square plate under equal biaxial compression loads in the x and y directions. Table 5 illustrates that the present N_{cr} values are identical to previous results by Ike (2023a), Hashemi et al (2016), Thai and Choi (2013).

Table 4 is used to calculate the percentage differences between the critical buckling load coefficients for simply supported plate under biaxial compressive load and the CPT results for various values of h/a as presented in Table 6.

The Table 6 shows that the percentage difference for $h/a = 0.01$ which is thin plate is zero, and the percentage difference increases with increasing h/a ratio to 22.50% for $h/a = 0.20$ (thick plate).

Similarly, Table 5 is used to compute the percentage differences between the critical buckling load coefficients for simply supported plate under biaxial buckling and CPT results for various values of h/a, as presented in Table 7.

Table 7 reveals that there is no difference between the present results and CPT results for $h/a = 0.01$ (thin plate) and the percentage difference increases with increase in h/a up to a percentage difference of 22.56% when $h/a = 0.20$ (thick plate). The difference between the present results and the CPT result is because the present result accounts for transverse shear deformation effects which are neglected in the CPT. This shows that transverse shear deformation decreases the buckling load capacity of thick plates, rendering the CPT unsafe for analysis and design of thick plates where transverse shear deformation plays significant role in their behavior.

6. Conclusion

This study has presented first principles formulation of thick plate buckling under uniaxial and biaxial compressive loads. The thick plate was modelled using trigonometric shear form functions to ensure the satisfaction of transverse shear strain-free conditions at the surfaces $z = \pm 0.5h$. The resulting system of two partial differential equations found from the vanishing of the first variation of the

total potential energy function was solved analytically using Galerkin variational method.

In conclusion,

(i) the critical buckling loads $N_{xx\,cr}$, $N_{yy\,cr}$, N_{cr} obtained for all values of a/h and b/a for uniaxial and biaxial cases are identical to results by Gunjal et al (2015), Reddy (1984), Mindlin (1951), Ike (2023a), Reddy and Phan (1985), and Deepak et al (2021).

(ii) when compared with present results, the CPT overestimates the $N_{xx\,cr}$, $N_{yy\,cr}$ for a/h = 5, and a/h = 10, which correspond to thick and moderately thick plates. The present $N_{yy\,cr}$ results for a/h = 5, b/a = 2 is 14.1% lower than the corresponding values for CPT.

(iii) the present results for N_{cr} for biaxial buckling for a/h = 5, are significantly different from CPT results with differences varying from 22.59% when b/a = 1 to 12.72% when b/a = 4.

(iv) the results for $N_{xx\,cr}$, $N_{yy\,cr}$, and N_{cr} for a/h = 50, and a/h = 100 (thin plates) do not differ greatly from the corresponding values obtained by the CPT, showing that the present formulation adequately captures thin plate buckling analysis.

(v) the significant differences existing in the present work for thick plates for which h/a = 0.20 and CPT results is attributed to the fact that the present work considers transverse shear deformation effect which is disregarded in the CPT, and this renders CPT unsuitable for buckling load analysis in thick plates.

Table 1

Dimensionless critical buckling loads $\hat{N}_{cr} = N_{xx_{cr}}$ for uniform uniaxial compression in the x-direction for simply supported rectangular plates $\mu = 0.30$, $E = 210$GPa

a/h	Theory/Reference	b/a						
		1	1.5	2	2.5	3	3.5	4
5	Present	2.949	1.621	1.237	1.075	0.991	0.942	0.911
	Gunjal et al (2015)	2.949	1.622	1.238	1.076	0.992	0.943	0.911
	Sayyad and Ghugal (2014)	3.026	1.654	1.259	1.093	1.007	0.957	0.925
	Reddy (1984)	2.951	1.621	1.237	1.075	0.991	0.942	0.911
	Mindlin (1951)	2.949	1.621	1.237	1.075	0.991	0.942	0.911
	CPT (Gunjal et al, 2015)	3.615	1.885	1.412	1.216	1.115	1.057	1.020
10	Present	3.422	1.811	1.364	1.177	1.081	1.026	0.990
	Gunjal et al (2015)	3.422	1.812	1.364	1.178	1.082	1.026	0.911
	Sayyad and Ghugal (2014)	3.454	1.825	1.373	1.185	1.089	1.032	0.997
	Reddy (1984)	3.422	1.812	1.364	1.177	1.081	1.026	0.990
	Mindlin (1951)	3.422	1.811	1.364	1.177	1.081	1.026	0.990
	CPT (Gunjal et al, 2015)	3.615	1.885	1.412	1.216	1.115	1.057	1.020
20	Present	3.564	1.866	1.399	1.206	1.107	1.049	1.012
	Gunjal et al (2015)	3.565	1.867	1.400	1.206	1.107	1.049	1.013
	Sayyad and Ghugal (2014)	3.582	1.874	1.405	1.211	1.111	1.053	1.016
	Reddy (1984)	3.564	1.866	1.399	1.206	1.107	1.049	1.012
	Mindlin (1951)	3.564	1.866	1.399	1.206	1.107	1.049	1.012

	CPT (Gunjal et al, 2015)	3.615	1.885	1.412	1.216	1.115	1.057	1.020
50	Present	3.607	1.882	1.410	1.214	1.114	1.056	1.019
	Gunjal et al (2015)	3.607	1.883	1.412	1.216	1.114	1.057	1.020
	Sayyad and Ghugal (2014)	3.621	1.889	1.415	1.219	1.118	1.059	1.022
	Reddy (1984)	3.607	1.882	1.410	1.214	1.114	1.055	1.018
	Mindlin (1951)	3.607	1.882	1.410	1.214	1.114	1.056	1.019
	CPT (Gunjal et al, 2015)	3.615	1.885	1.412	1.216	1.115	1.057	1.020
100	Present	3.613	1.885	1.411	1.215	1.115	1.057	1.020
	Gunjal et al (2015)	3.613	1.885	1.412	1.216	1.115	1.057	1.020
	Sayyad and Ghugal (2014)	3.625	1.891	1.416	1.219	1.115	1.060	1.023
	Reddy (1984)	3.613	1.884	1.411	1.215	1.115	1.056	1.019
	Mindlin (1951)	3.613	1.885	1.411	1.215	1.115	1.057	1.020
	CPT (Gunjal et al, 2015)	3.615	1.885	1.412	1.216	1.115	1.057	1.020

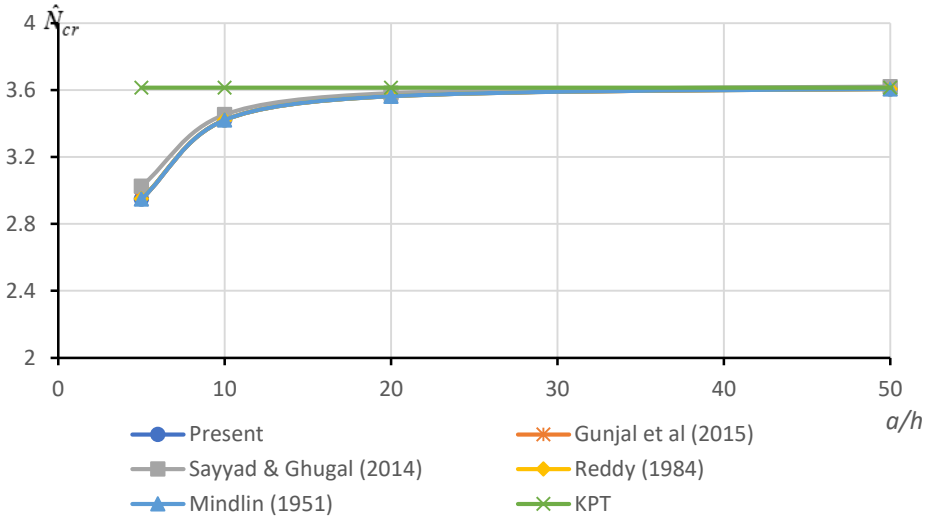

Figure 3: Graph of $\hat{N}_{cr}$ vs a/h for square plate under uniform uniaxial compression in the x-direction (for critical buckling load)

Table 2

Dimensionless critical buckling loads $\hat{N}_{cr} = N_{yy_{cr}}$ for simply supported rectangular plates under uniform compression in the y-direction $\mu = 0.30$, $E = 210\text{GPa}$

a/h	Theory/Reference	b/a						
		1	1.5	2	2.5	3	3.5	4
5	Present	2.949	3.648	4.950	6.721	8.923	11.545	14.578
	Gunjal et al (2015)	2.949	3.650	4.953	6.724	8.927	11.549	14.583
	Sayyad and Ghugal (2014)	3.026 (2.61%)	3.721 (2%)	5.039 (1.8%)	6.835 (1.7%)	9.069 (1.64%)	11.729 (1.59%)	16.269 (1.16%)
	Reddy (1984)	2.951	3.649	4.951	6.722	8.925	11.546	14.580
	Mindlin (1951)	2.949	3.648	4.950	6.721	8.923	11.545	14.578
	CPT (Gunjal et al, 2015)	3.615	4.242	5.648	7.601	10.042	12.953	16.325
10	Present	3.442	4.076	5.456	7.360	9.737	12.570	15.850

	Gunjal et al (2015)	3.442	4.077	5.457	7.361	9.738	12.570	15.851
	Sayyad and Ghugal (2014)	3.424 (0.82%)	4.108 (0.79%)	5.495 (0.71%)	7.410 (0.68%)	9.802 (0.67%)	12.652 (0.65%)	15.953 (0.65%)
	Reddy (1984)	3.422	4.076	5.456	7.360	9.737	12.570	15.850
	Mindlin (1951)	3.422	4.076	5.456	7.360	9.737	12.570	15.850
	CPT (Gunjal et al, 2015)	3.615	4.242	5.648	7.601	10.042	12.953	16.325
20	Present	3.564	4.20	5.599	7.539	9.964	12.855	16.204
	Gunjal et al (2015)	3.565	4.20	5.60	7.539	9.964	12.855	16.204
	Sayyad and Ghugal (2014)	3.582	4.218	5.623	7.57	10.005	12.907	16.269
	Reddy (1984)	3.564	4.2	5.599	7.539	9.964	12.855	16.204
	Mindlin (1951)	3.564	4.2	5.599	7.539	9.964	12.855	16.204
	CPT (Gunjal et al, 2015)	3.615	4.242	5.648	7.601	10.042	12.953	16.325
50	Present	3.607	4.236	5.641	7.591	10.030	12.953	16.325
	Gunjal et al (2015)	3.607	4.236	5.641	7.591	10.030	12.937	16.306
	Sayyad and Ghugal (2014)	3.621	4.251	5.660	7.618	10.066	12.984	16.365
	Reddy (1984)	3.606	4.235	5.640	7.590	10.028	12.935	16.303
	Mindlin (1951)	3.607	4.236	5.641	7.591	10.030	12.953	16.325
	CPT (Gunjal et al, 2015)	3.615	4.242	5.648	7.601	10.042	12.953	16.325
100	Present	3.613	4.241	5.646	7.598	10.037	12.950	16.321
	Gunjal et al (2015)	3.613	4.241	5.647	7.599	10.039	12.9490	16.32
	Sayyad and Ghugal (2014)	3.625	4.255	5.665	7.624	10.073	12.992	16.375
	Reddy (1984)	3.613	4.24	5.646	7.595	10.037	12.944	16.312
	Mindlin (1951)	3.613	4.241	5.646	7.598	10.037	12.95	16.321
	CPT (Gunjal et al, 2015)	3.615	4.242	5.648	7.601	10.042	12.953	16.325

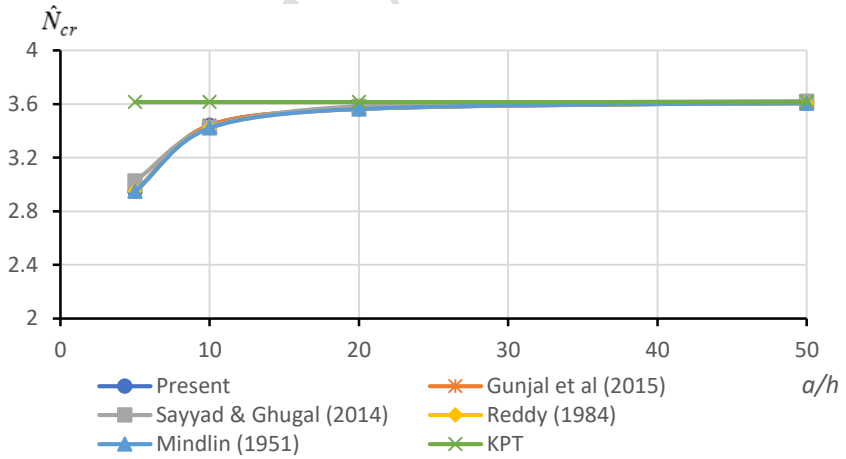

Figure 4: Graph of $\hat{N}_{cr}$ vs a/h for square plate under uniaxial uniform compression in the y-direction (for critical buckling load)

Table 3

Dimensionless critical buckling loads $\hat{N}_{cr} = N_{xxyy_{cr}}$ for simply supported isotropic rectangular plates subjected to biaxial compressive forces $\mu = 0.30$, $E = 210\text{GPa}$, $\hat{N}_{cr} = \dfrac{N_0 a^2}{Eh^3}$

a/h	Theory/Reference	b/a						
		1	1.5	2	2.5	3	3.5	4
5	Present	1.474	1.122	0.99	0.927	0.892	0.871	0.857
	Gunjal et al (2015)	1.475	1.123	0.991	0.927	0.893	0.872	0.858
	Sayyad and Ghugal (2014)	1.513	1.145	1.007	0.942	0.907	0.885	0.871
	Reddy (1984)	1.475	1.122	0.99	0.927	0.892	0.871	0.857
	Mindlin (1951)	1.474	1.122	0.99	0.927	0.892	0.871	0.857
	CPT (Gunjal et al, 2015)	1.807	1.305	1.129	1.048	1.004	0.977	0.960
10	Present	1.711	1.254	1.091	1.015	0.973	0.948	0.932
	Gunjal et al (2015)	1.711	1.254	1.091	1.015	0.974	0.949	0.932
	Sayyad and Ghugal (2014)	1.727	1.264	1.099	1.022	0.980	0.954	0.938
	Reddy (1984)	1.711	1.254	1.091	1.015	0.973	0.948	0.932
	Mindlin (1951)	1.711	1.254	1.091	1.015	0.973	0.948	0.932
	CPT (Gunjal et al, 2015)	1.807	1.305	1.129	1.048	1.004	0.977	0.96
20	Present	1.782	1.292	1.119	1.039	0.996	0.970	0.953
	Gunjal et al (2015)	1.783	1.292	1.120	1.04	0.996	0.97	0.953
	Sayyad and Ghugal (2014)	1.791	1.298	1.124	1.045	1.00	0.974	0.957
	Reddy (1984)	1.782	1.292	1.119	1.039	0.996	0.97	0.953
	Mindlin (1951)	1.782	1.292	1.119	1.039	0.996	0.970	0.953
	CPT (Gunjal et al, 2015)	1.807	1.305	1.129	1.048	1.004	0.977	0.96
50	Present	1.803	1.303	1.128	1.046	1.002	0.976	0.959
	Gunjal et al (2015)	1.804	1.303	1.128	1.047	1.003	0.976	0.959
	Sayyad and Ghugal (2014)	1.810	1.308	1.132	1.050	1.006	0.979	0.962
	Reddy (1984)	1.803	1.303	1.128	1.046	1.002	0.976	0.959
	Mindlin (1951)	1.803	1.303	1.128	1.046	1.002	0.976	0.959
	CPT (Gunjal et al, 2015)	1.807	1.305	1.119	1.048	1.004	0.977	0.96
100	Present	1.806	1.305	1.129	1.048	1.003	0.977	0.96
	Gunjal et al (2015)	1.807	1.305	1.129	1.048	1.004	0.977	0.96
	Sayyad and Ghugal (2014)	1.812	1.309	1.133	1.051	1.007	0.98	0.963
	Reddy (1984)	1.806	1.304	1.129	1.048	1.003	0.977	0.96
	Mindlin (1951)	1.806	1.305	1.129	1.048	1.003	0.977	0.96
	CPT (Gunjal et al, 2015)	1.807	1.305	1.129	1.048	1.004	0.977	0.96

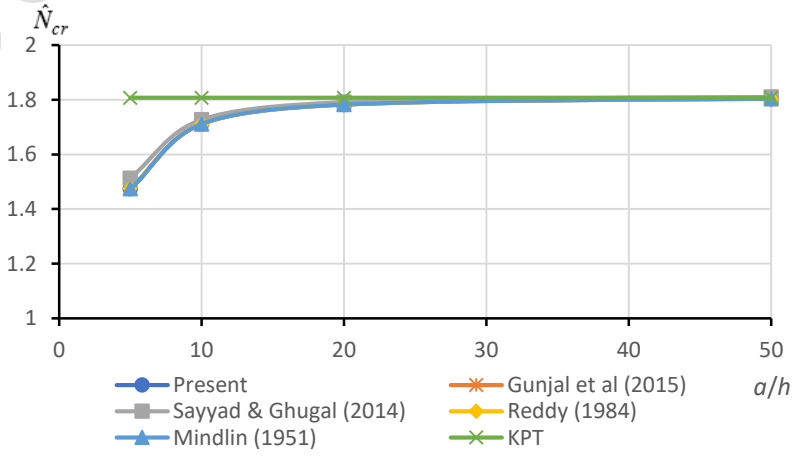

Figure 5: Variation of $\hat{N}_{cr}$ with a/h for biaxially compressed square plate (for critical buckling load)

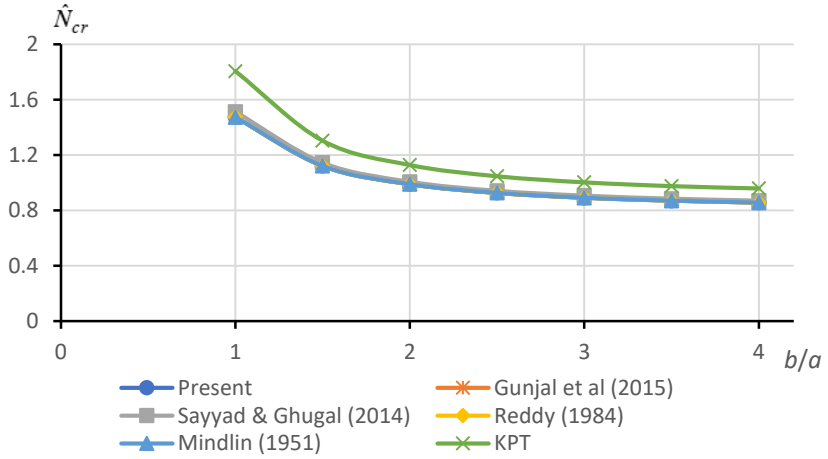

Figure 6: Variation of $\hat{N}_{cr}$ with b/a for biaxially compressed square plate for a/h = 5 (for critical buckling mode)

Table 4: Critical buckling load coefficients of a simply supported square plate under uniform uniaxial compression load (for $\mu = 0.30$), $E = 210\text{GPa}$, $\bar{N}_{cr} = \dfrac{N_0 a^2}{\pi^2 D}$

	$N_{xx} = -N_0,\ N_{yy} = 0,\ N_{xy} = 0$			
Reference/Theory	h/a = 0.01	h/a = 0.05	h/a = 0.10	h/a = 0.20
Present study	4.0000	3.9443	3.7865	3.2653
SVPBT (Ike, 2023a)	4.0000	3.9444	3.7864	3.2637
Mindlin (Hashemi et al, 2008)	4.0000	3.9444	3.7864	3.2637
RPT (Thai and Choi, 2013)	4.0000	3.9443	3.7865	3.2653
Exact (Srivinas and Rao, 1969)	4.0000	3.9110	3.7410	3.1500
Reddy (Reddy and Phan, 1985)	–	3.9443	3.7865	3.2653
SVSPT (Deepak et al, 2021)	4.0000	3.9444	3.7864	3.2637
CPT (Timoshenko and Gere, 1961)	4.0000	4.0000	4.0000	4.0000

Table 5: Critical buckling load coefficients of a simply supported square plate under uniform biaxial compression load (for $\mu = 0.30$), $E = 210\text{GPa}$, $\bar{N}_{cr} = \dfrac{N_0 a^2}{\pi^2 D}$

	$N_{yy} = N_{xx} = -N_0 (N_{xy} = 0)$			
Reference/Theory	h/a = 0.01	h/a = 0.05	h/a = 0.10	h/a = 0.20
Present study	2.0000	1.9722	1.8932	1.6319
SVPBT (Ike, 2023a)	2.0000	1.9722	1.8932	1.6319
Mindlin (Hashemi et al, 2008)	2.0000	1.9722	1.8932	1.6319
RPT (Thai and Choi, 2013)	2.0000	1.9722	1.8932	1.6327
Reddy (Reddy and Phan, 1985)	2.0000	1.9722	1.8933	1.6327
SVSPT (Deepak et al, 2021)	2.0000	1.9722	1.8932	1.6312

Exact (Srivinas and Rao, 1969)	–	–	–	–
CPT (Timoshenko and Gere, 1961)	2.0000	2.0000	2.0000	2.0000

Table 6: Percentage differences between the present critical buckling load coefficients results for simply supported square plate under uniaxial compressive load and CPT results for various values of *h*/*a*

h/*a*	0.01	0.05	0.10	0.20
% Difference	0%	1.41%	5.64%	22.50%

Table 7: Percentage differences between the present critical buckling load coefficients results for simply supported square plate under biaxial compressive load and CPT results for various values of *h*/*a*

h/*a*	0.01	0.05	0.10	0.20
% Difference	0%	1.41%	5.64%	22.56%

Table 8: Dimensionless critical buckling load parameters, $\bar{N}$ of square plates subjected to uniform tensile load in the *x* direction and compressive load in the *y* direction for $\mu = 0.30$, $E = 210$, for $a/h = 5,\ 10, 20, 50, 100$

$$\bar{N} = \frac{N_{cr}a^2}{Eh^3}$$

a/*h*	Modles		$\bar{N}$
5	Present study		4.8274
	4VRPT Bonrado et al (2016)		4.8274
	RPT Kim et al (2009)		4.8274
	FSDT Kim et al (2009)		4.8158
	CPT		7.5317
10	Present study		6.6024
	4VRPT Bonrado et al (2016)		6.6024
	RPT Kim et al (2009)		6.6024
	FSDT Kim et al (2009)		6.6010
	CPT		7.5317
20	Present study		7.2754
	4VRPT Bonrado et al (2016)		7.2754
	RPT Kim et al (2009)		7.2754
	FSDT Kim et al (2009)		7.2753
	CPT		7.5317
50	Present study		7.4895
	4VRPT Bonrado et al (2016)		7.4895
	RPT Kim et al (2009)		7.4895
	FSDT Kim et al (2009)		7.4895
	CPT		7.5317
100	Present study		7.5211
	4VRPT Bonrado et al (2016)		7.5211
	RPT Kim et al (2009)		7.5211
	FSDT Kim et al (2009)		7.5211

	CPT		7.5317

Table 8 shows that the present results for dimensionless critical buckling load parameters for square plate under tension in x direction and compression load in the y direction are in excellent agreement with previously computed values of Kim et al (2009) using two-variable refined plate theory (2VRPT) and FBDPT for $k_c = 5/6$ for values of $a/h = 5,\ 10,\ 20,\ 50$ and 100. The least buckling loads occur when the buckling modes are $m = 1,\ n = 2$ for the present study and previous studies by Kim et al (2009). Table 8 also shows that the CPT results are the same irrespective of the value of a/h and CPT overestimates the critical buckling load by 56.02% when $a/h = 5$ by 14.08% when $a/h = 10$, and by 3.52% when $a/h = 20$.

References

Bacciocchi M., Tarantino A.C. (2021) "Third-order theory for the bending analysis of laminated thin and thick plates including the strain gradient effect" Materials, 14(7), 1771. https://doi.org/10.3390/ma1407177.

Bourada, F., Amara, K. and Tounsi, A. (2016). "Buckling analysis of isotropic and orthotropic plates using a novel four variable refined plate theory," *Steel and Composite Structures*, 21(6), 1287 – 1306. https://doi.org/10.12989/SCS.2016.21.6.1287

Deepak, S.A., Shetty, R.A., Sudheer, K.K. and Dushyanthkumar, G.L. (2021). "Buckling analysis of thick plates using a single variable simple plate theory," *Journal of Mines, Metals and Fuels*, 2021(2021), 67 – 72.

Deepak, S.A., Shetty, R.A., Sudheer, K.K. and Dushyanthkumar, G.L. (2022). "Buckling analysis of thick plates using a single variable simple plate theory," *Journal of Mines, Metals and Fuels*, 69(12A), 67 – 72. https://doi.org/10.18311/jmmf/2021/30097

Fu W. and Wang B. (2022). "A semi-analytical model on the critical buckling load of perforated plates with opposite free edges." Proceedings of Institution of Mechanical Engineers. Journal of Mechanical Engineering Science 236(9), 4885-4894. https://doi.org/10.1177/09544062211056890.

Gajbhiye, P.D., Bhaiya, V. and Ghugal, Y.M. (2022). "Buckling analysis of thick plates using 5th order shear deformation theory," In: Singh, S.B., Barai, S.V. (eds) *Stability and Failure of High Performance Composite Structures*. Composite Science and Technology, Springer, Singapore. https://doi.org/10/1007/978-981-19-2424-8_19.

Godwin G., Onodagu D.P., Ezeagu A.C. (2023). "Buckling analysis of thick isotropic rectangular SSFS plates using polynomial displacement functions." UNIZIK Journal of Engineering and Applied Sciences 2(3), 285 – 297. https://journals.unizik.edu.ng/index.php/ijeas.

Gunjal, S.M., Hajare, R.B., Sayyad, A.S. and Ghodle, M.D. (2015). "Buckling analysis of thick plates using refined trigonometric shear deformation theory," *Journal of Materials and Engineering Structures*, 2(2015), 159 – 167.

Hashemi S.H., Korshidi K., Amabili M. (2008). "Exact solutions for linear buckling of rectangular Mindlin plates." *Journal of Sound and Vibration*, 315(2008), 318 – 342. https://dx.doi.org/1016/j.jsv.2008.01.059.

Hassan A. and Kurgan N. (2019). "Modeling and Buckling Analysis of Rectangular Plates in ANSYS" International Journal of Engineering and Applied Sciences 11(1), 310 – 329. https://dx.doi.org/10.24107/ijeas.531011.

Ike, C.C. (2023a). "Single variable thick plate buckling problems using double finite sine transform method," *Engineering and Technology Journal*, 41(11), 1403 – 1413. https://doi.org/10.30684/etj.203.1425044.1537

Ike, C.C. (2023b). "A third-order shear deformation plate bending formulation for thick plates: first principles derivation and applications," *Mathematical Models in Engineering*, 9(4), 144 – 168. https://doi.org/10.21595/mme.2023.23688

Ike, C.C. (2025a). "Double Fourier series method for bending solutions of simply supported Mindlin plates," *Civil Engineering Infrastructures Journal*, Articles in Press: https://doi.org/10.22059/ceij/2025.374673.2041

Ike, C.C. (2025b). "Ritz variational method for the exact bending analysis of clamped Mindlin plates," *NIPES – Journal of Science and Technology Research*, 7(1), 219 – 234. https://doi.org/10.37933/nipes/7.1.2025.18.

Ike, C.C. (2025c). "Buckling analysis of relatively thick plates using first order shear deformation plate theory: Exact solutions," *NIPES – Journal of Science and Technology Research*, 7(2), 23 – 43. https://doi.org/10.37933/nipes.7.2.2025.2

Ike C.C. (2025d). "Analysis of single variable thick plate buckling problems using Galerkin method" NIPES-Journal of Science and Technology Research 7(2), 235 – 252. https//doi.org/10.37933/nipes/7.2.2025.16.

Ike C.C. (2025e). "Variational formulations of exponential shear deformable plate buckling problems and analytical solutions using double Fourier series method" NIPES-Journal of Science and Technology Research 7(3), 1 – 18. https//doi.org/10.37933/nipes/7.3.2025.3.

Jayabalan J., Dominic M., Ebid A.M., Soleymani A., Onyelowe K.C. and Jahangir H. (2022). "Estimating the buckling load of steel plates with center cut-outs by ANN, GET and EPR techniques." Designs 6(5), 84. https://doi.org/10.33906050084.

Khalfi, Y., Sallai, B. and Bellebna, Y. (2021). "Buckling analysis of plates using an efficient sinusoidal shear deformation theory," *Journal of Fundamental and Applied Sciences*, 14(1), 210 – 228. https://dx.doi.org/10.4314/jfas.v14i1.11.

Kim S.E., Thai H.T., Lee J. (2009b). Buckling analysis of plates using the two variable refined plate theory. Thin-Walled Structure 47(4), 455 – 462.

Kumar R. and Singh J. (2018). "Assessment of higher order transverse shear deformation theories for modelling and buckling analysis of FGM plates using RBF based meshless approach," *Multidiscipline Modelling in Materials and Structures*, 14(5), 891 – 907. https://doi.org/10.1108/mmms-07-2017.0069

Mindlin, R.D. (1951). Influence of rotatory inertia and shear deformation on flexural motion of isotropic, elastic plates. *Journal of Applied Mechanics, 18*, 31 – 38. https://doi.org/10.1115/1.4010217

Mohseni E. and Naderi A. (2023). "Effect of higher order shear and normal deformable theory in buckling analysis of thick porous functionally graded plates" Journal of Computational Applied Mechanics 54(3), 347 – 364. https://doi.org/10.22059/jcamech.2023.361677.852.

Moslemi, A., Neya, B.N. and Amiri J.V. ((2016a) "3-D elasticity buckling solution for simply supported thick rectangular plates using displacement potential functions." *Applied Modelling* 40(11), 5717-5730. DOI:10.1016/j.apm.2015.12.034.

Moslemi, A., Neya, B.N., Amiri, J.V. (2016b). "Benchmark solution for buckling thick rectangular transversely isotropic plates under biaxial load." *International Journal of Mechanical Sciences,* 131-132(2016), 356-367. https://doi.org/10.1016/j.ijmecsi.2017.006

Onodagu D.P., Ezeagu A.C., Godwin G. (2023). "Buckling analysis of thick isotropic rectangular SSSS plates using Ritz method in polynomial displacement functions." Nnamdi Azikiwe University Journal of Civil Engineering 1(4), 14 – 23. www.naujeve.com.

Onyeka, F.C., Mama, B.O. and Okeke, T.E. (2022). "Exact three dimensional stability analysis of plate using a direct variational energy method," *Civil Engineering Journal (Iran)*, 8(1), 60 – 80. DOI:10.28991/CEJ-2022-08-01-05.

Prabowo, A.R.; Ridwan, R.; Muttaqie T. (2022). "On the resistance to buckling loads of idealized hull structures: FE analysis on designed – stiffened plates" Designs 2022, 6, 46. https://doi.org/10.3390/designs6030046.

Reddy J.N., Phan N.D. (1985). "Stability and vibration of isotropic, orthotropic and laminated plates according to a higher-order shear deformation theory." *Journal of Sound and Vibration*, 98(1985), 158 – 170. https://doi.org/10.1016/0022-460X(85)90383-9

Reddy, J.N. (1984). "A simple higher order theory for laminated composite plates," *ASME Journal of Applied Mechanics*, 51(1984), 745 – 752.

Sayyad, A.S. and Ghugal, Y.M. (2014). "On the buckling of isotropic, transversely isotropic and laminated composite rectangular plates," *International Journal of Structural Stability and Dynamics*, 14(7), 1 – 32.

Sayyad I., Thakur A.G., Bhaskar D.P. (2022). "Plate Structure Buckling Analysis using Refined Theory" NeuroQuantology 20(16), 4239-4252. https://doi.org/10.48047/NQ.2022.20.16.NQ880433.

Shaban M., Khoshgoftar M.J. (2023). "Closed-form formulation for bending analysis of functionally graded thick plates" Journal of Solid Mechanics 15(2), 160 – 173. https://doi.org/10.22034/jsm.2023.1973962.1758.

Shimpi, R.P., Guruprasad, P.J. and Pakhare, K.J. (2018). "Single variable new first order shear deformation theory for isotropic plates," *Latin American Journal of Solids and Structures*, 15(2018)e124, 1 – 25. https://doi.org/10.1590/1679-78254842

Srinivas S., Rao A.K. (1969). Buckling of thick rectangular plates. *AIAA Journal*, 7(1969), 1645 – 1646.

Su H., Bai E., Hai G. (2023). "Unified solution of some problems of rectangular plates with four free edges based on symplectic superposition method." *Engineering Computations*, 40(6), 1330 – 1350. https://doi.org/10.1108/EC-08-2022-0533

Thai H.T., Choi D.H. (2013). "Analytical solutions of refined plate theory for bending, buckling and vibration analysis of thick plates." *Applied Mathematical Modelling*, 37(2013), 8310 – 8323. https://doi.org/10.1016/j.apm.2013.03.038

Timoshenko, S.P., Gere, G.M. (1961). Theory of Elastic Stability. 2nd Edition, McGraw Hill Book Company, New York.

Ullah S., Zhong J., Zhong Y. (2019). "New analytical solutions of buckling problems of rotationally restrained rectangular thin plates." *International Journal of Applied Mechanics*, Vol 11, No. 10, pp 1950101.

Wang Y.W., Long F., Li XF (2025) "A novel single-variable third-order shear deformation theory for free vibration of rectangular plates" Acta Mechanica https://doi.org/10.1007/s00707-025-04504-5.

Zargaripoor, A., Bahrami, A. and Nikkah B.M. (2018). "Free vibration and buckling analysis of third order shear deformation plate theory using exact wave propagation approach," *Journal of Computational Applied Mechanics*, 49(1), 102 – 124. DOI:10.22059/jcamech.2018.249468.227.